ATC 施設利用・共同開発研究　成果報告書

国立天文台先端技術センター　センター長　常田 佐久　殿　　　　　　　　　平成 29 年 4 月 3 日

下記のとおり施設利用の成果を報告します。

ふりがな：　　　もとはらけんたろう 代表者氏名：本原顕太郎	③所属機関，部局： 東京大学・天文学教育研究センター

研究課題名：TAO6.5m 望遠鏡用近赤外線分光カメラ SWIMS の開発

利用期間：Ｈ２８年　４月　１日　～　Ｈ２９年　３月３１日

利用者リスト
　尾崎忍夫、田中培生、加藤夏子、本原顕太郎、高橋英則、小西真広、北川祐太朗、寺尾恭範、大橋宗史

研究開発の成果（ATC 施設利用との関連を具体的に記述してください。）
現在東京大学天文学研究センターは、南米チリ・アタカマのチャナントール山頂に６．５ｍの大型赤外線望遠鏡の建設を進めている。
我々のグループではその第一期観測装置の一つである SWIMS の開発を行っている。
今年度は、以下の様な先端技術センターと関連した活動を行った。

- 総合冷却試験：継続して全コンポーネントをインストールした総合冷却試験を４回行い、検出器焦点位置などの最終調整を行った。この際、予冷に用いる液体窒素（一回あたりおよそ 500l）の提供を受けた。
- フィルター試験：納入された狭帯域フィルタの透過率測定を SolidSpec370 を用いて、および表面形状測定を Zygo 干渉計を用いて行った。
- 機械加工：SWIMS の完成に向けて、細かな部品の最適化加工や、各種試験に必要な治具などの製作を、マシンショップの機械を利用して行った。

施設利用が謝辞等に記された学術論文など（資料を添付してください。）

- Motohara et al., Proc. SPIE 9908, 99083U (2016)
- Terao et al., Proc. SPIE 9915, 99151W (2016)
- Kitagawa et al., Proc. SPIE 9912, 991225 (2016)

先端技術センターの利用設備・実験室等の利用した物品を具体的に記入してください。マシンショップへ依頼したリスト・利用した測定器・CAD 等について記入してください。）

- 液体窒素：2000l 程度
- オプトショッ：Zygo GPI, SolidSpec370
- マシンショップ工作加工(申請者との共同加工も含む)
  - ✓ 検出器熱パスの部品製作（工作機械利用）

先端技術センターの施設への要望等ありましたら、記入してください。

毎度のことですが、使用頻度は低いものの重要な測定機器などをしっかりメンテナンスされながら維持していただいているのと同時に、各種加工の相談に乗っていただくなど、大学での装置開発にとっては欠かすことのできない施設です。今後も、この機能を維持していただけるよう期待しております。

NIR camera and spectrograph SWIMS for TAO 6.5m telescope : Overview and development status

Kentaro Motohara[a], Masahiro Konishi[a], Hidenori Takahashi[a], Natsuko M. Kato[a], Yutaro Kitagawa[a], Yutaka Kobayakawa[a], Yasunori Terao[a], Hirofumi Ohashi[a], Tsutomu Aoki[b], Mamoru Doi[a,c], Takafumi Kamizuka[a], Kotaro Kohno[a], Takeo Minezaki[a], Takashi Miyata[a], Tomoki Morokuma[a], Kiyoshi Mori[a], Ryou Ohsawa[a], Kazushi Okada[a], Shigeyuki Sako[a], Takao Soyano[b], Yoichi Tamura[a], Toshihiko Tanabe[a], Masuo Tanaka[a], Ken'ichi Tarusawa[b], Masahito S Uchiyama[a], Shintaro Koshida[d], Kentaro Asano[e], Ken Tateuchi[a], Mizuho Uchiyama[f], Soya Todo[a], and Yuzuru Yoshii[a]

[a]Institute of Astronomy, Graduate School of Science, The University of Tokyo, 2-21-1 Osawa, Mitaka Tokyo 181-0015, Japan
[b]Kiso Observatory, Institute of Astronomy, Graduate School of Science, The University of Tokyo, 10762-30 Mitake, Kiso, Nagano 397-0101, Japan
[c]Research Center for the Early Universe, Graduate School of Science, The University of Tokyo, 7-3-1 Hongo, Bunkyo-ku, Tokyo 113-0033, Japan
[d]Subaru Telescope, National Astronomical Observatory of Japan, 650 North A'ohoku Place, Hilo, HI 96720, USA
[e]Institute of Space and Astronautical Science,Yoshinodai 3-1-1, Chuo-ku, Sagamihara, Kanagawa 252-5210, Japan
[f]National Astronomical Observatory of Japan, 2-21-1 Osawa, Mitaka Tokyo 181-8588

ABSTRACT

Simultaneous-color Wide-field Infrared Multi-object Spectrograph, SWIMS, is one of the first generation instruments for University of Tokyo Atacama Observatory 6.5m Telescope where almost continuous atmospheric window from 0.9 to 2.5μm appears, thanks to the high altitude and dry climate of the site. To utilize this excellent condition, SWIMS is capable of simultaneous two-color imaging with a field of view of $9^{'}.6$ in diameter and $\lambda/\Delta\lambda \sim 1000$ multi-object spectroscopy at 0.9–2.5μm in a single exposure, utilizing a dichroic mirror inserted in the collimated beam. Here, we overview the instrument, report results of its full-assembly tests in the laboratory and present the future plan.

Keywords: near infrared, mutli-object spectroscopy, wide field imager, integral field unit, TAO 6.5m telescope

1. INTRODUCTION

Observations in the infrared wavelengths beyond $\sim$1μm at ground-based telescopes suffer from atmospheric absorption by various terrestrial molecules, such as water vapor, ozone, and carbon dioxide, which cause deep absorption bands. To avoid them, one of the best way is to go to higher altitude where especially the water vapor is well suppressed. University of Tokyo Atacama Observatory (TAO) 6.5m telescope project(PI: Yuzuru Yoshii[1–3]) is to construct an infrared-optimized telescope at the summit of Co. Chajnantor in northern Chile. In combination of its high altitude of 5640m, with the dry climate of the site (precipitable water vapor : PWV$\sim$0.5mm), the atmospheric absorption by water vapor is reduced and we can carry out observation in wavelengths up to 38μm, which cannot be done at other existing sites.[4,5]

Further author information: (Send correspondence to K.M.)
K.M. : E-mail: kmotohara@ioa.s.u-tokyo.ac.jp, Telephone: 81 422 34 5163

Ground-based and Airborne Instrumentation for Astronomy VI, edited by Christopher J. Evans, Luc Simard, Hideki Takami
Proc. of SPIE Vol. 9908, 99083U · © 2016 SPIE · CCC code: 0277-786X/16/$18 · doi: 10.1117/12.2231386

In the near infrared wavelength of 0.9–2.5μm, the absorption bands separating atmospheric windows of the Y, J, H, and K-bands becomes much weaker at the TAO site, and observable wavelength rages are widen, therefore we can stably observe hydrogen Paschen-α emission line at 1.875μm[6–8] in the local universe, as well as other redshifted emission lines from distant galaxies. Simultaneous-color Wide-field Infrared Multi-object Spectrograph, SWIMS, is one of the first generation instruments for the TAO 6.5m telescope. It is capable of multi-object spectroscopic observations, obtaining full spectra from 0.9 to 2.5μm in a single exposure with $\lambda/\Delta\lambda \sim 1000$, as well as wide-field imaging with a field of view (FoV) of $9'.6$ in diameter, to make the best use of the characteristics of the site.

In this paper, we present overview of SWIMS and its current development status.

2. INSTRUMENT OVERVIEW

The main cryostat dewar of SWIMS has a cylindrical shape of 1.5m in height and 1.3m in diameter, and cooled down below 100K with a single GM-cycle cooler. The dewar is contained in a box of 2m $\times$ 2m $\times$ 2m, and its total weight is approximately 2.5ton. The whole instrument will be installed on the Nasmyth focus of the TAO 6.5m telescope with an instrument rotator. Figure 1 shows SWIMS fully assembled and under cool-down test in Japan. Detailed design and description of the SWIMS dewar and optics are presented in Konishi et al. (2012)[9] and Motohara et al. (2014).[10]

Figure 2 shows the layout of the optics inside the dewar. A dichroic mirror is inserted in a collimated beam to split it into two arms, the blue-arm covering 0.9–1.45μm and the red-arm 1.45–2.5μm. Thus, SWIMS is capable of two-color simultaneous imaging or $\lambda/\Delta\lambda \sim 1000$ multi-object spectroscopy at 0.9–2.5μm wavelength range with a single exposure, and enables us to carry out efficient NIR imaging/spectroscopic surveys. Each arm has three filter wheels, two for broad-band filters containing seven filters/grism each, and one for narrow-band filters containing six filters. The focal plane of each arm is designed to be covered by four HAWAII-2RGs arrays,

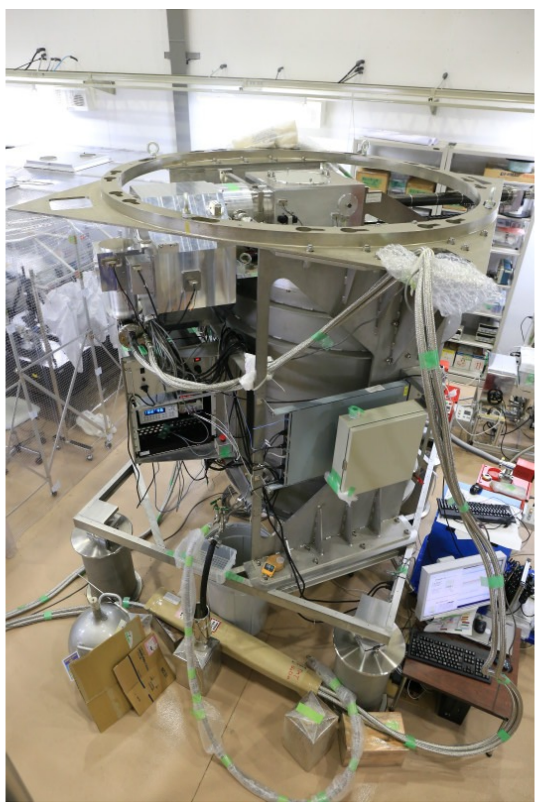

Figure 1. SWIMS fully assembled and under cooling test in a laboratory at Mitaka, Japan.

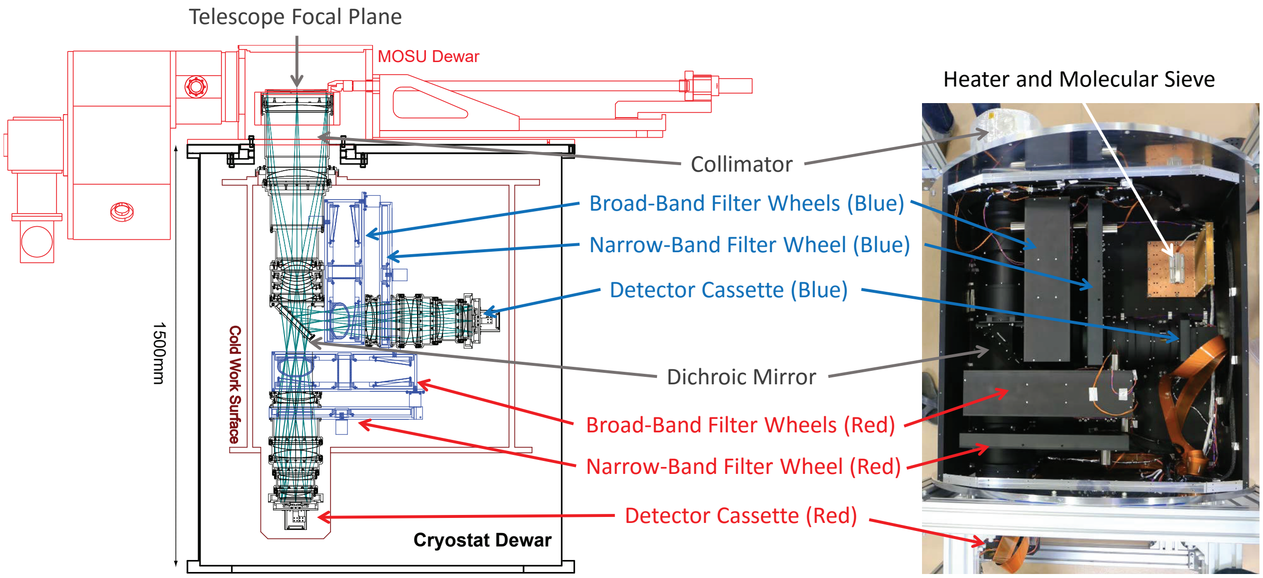

Figure 2. (Left) Overall schematics inside the dewar of SWIMS. (Right) All the components fully assembled on the cold work surface.

however, currently only two arrays each are procured which provide FoV of $8'\!.6 \times 4'\!.3$, with a pixel scale of $0''\!.126$.

The telescope focal plane is covered by a separate dewar for a multi-object slit mask exchanger unit (MOSU), which has a carousel to store multi-object slits (MOS) masks and a gate valve to separate the main dewar from the MOSU dewar.[11] MOS masks cover $5' \times 8'\!.6$, and maximum $\sim$30 slits with length of $15''$can be arranged on it. The masks are installed in a rotating carousel in the MOSU dewar which can store maximum 20 of them, and a robotic arm place one of it at the focal plane / house it into the carousel.

An IFU module covering $17'' \times 13''$with 26 slitlets of $0''\!.5$ width are also being developed.[12–14] The module is designed to be compact enough that it can be stored in the MOSU carousel and can be handled by the robotic arm as well.

Detailed information on the current status of the detector and its control system and the IFU module is reported elsewhere.[12,15]

3. SOFTWARE AND CONTROLS

SWIMS is controlled by a dedicated software, Instrument Control System (ICS), running on a Linux PC called OBCP. To make the ICS highly compatible with the observation control system of the Subaru telescope called Gen2,[16] we slightly modify the interface design of the ICS described in Motohara et al. (2014). Figure 3 outlines the current ICS layout together with the hardware layout. We merge the top-level module being called "Task Manager" into a Gen2 interface module (*g2cam*) as an instrument management server. The management server runs as an asynchronous socket server, in which a command issued by a user is sent in an appropriate manner to a TCP/IP socket server corresponding to a device called *device manager*. We prepare following *device managers* which are closely related to observations: `MOSU`, `Wheel`, `DET_B`, and `DET_R`. Synchronous exposures of the multiple detector arrays in each arm are coordinated by the management server. Synchronization between the two arms is handled in the Gen2. Each *device manager* has two independent worker threads, `Executor` and `Interrupter`: the `Executor` handles normal operations such as motion controls in a one-by-one policy while the `Interrupter` takes care of interruptive or emergency operations. When the `Interrupter` executes a task to avoid an emergency

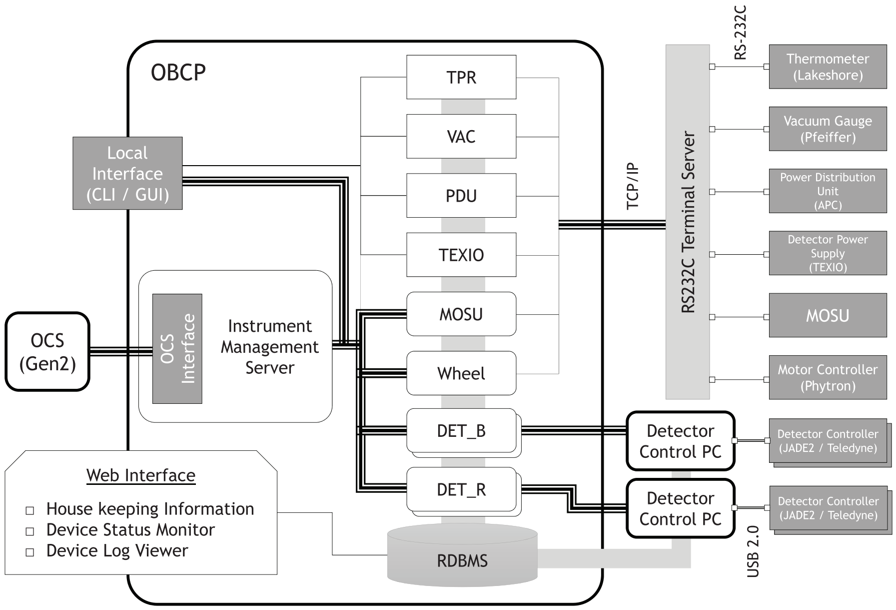

Figure 3. Control Software Diagram.

situation, all the normal commands in a waiting list of the `Executor` are discarded with an error notification for subsequent secure recovery operations. The *device manager*s are able to accept only pre-defined commands. For those hardware devices without *device manager*, we develop a command-line interface (CLI) which can be used both interactively in a stand-alone mode and as a Python module from the management server. Those CLIs will be also incorporated in graphical user interfaces (GUIs) in the future.

4. CRYOGENIC PERFORMANCE

In this section, we report results from the cooling test performed, and summarize the cryogenic performance.

4.1 Setup of Cryogenic Components

All the optical components are installed on the cold work-surface as shown in Figure 2. This work-surface is then installed on to the aluminum disk plate in the dewar jacket, called "diaphragm" to which a thermal path from a

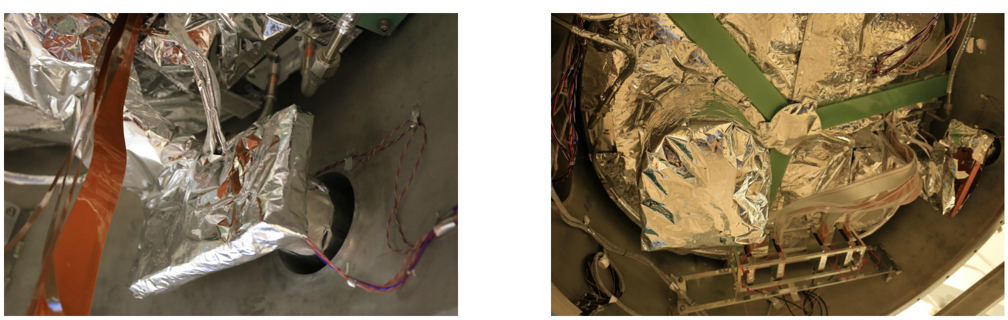

Figure 4. (Left) Thermal path connecting the cold head to the diaphragm, made of oxygen-free copper. Three more thermal paths from the center of rectangular block can be seen, which cool the detector cassettes and molecular sieve separately. (Right) The diaphragm, which hold the cold work-surface, seen from the bottom of the dewar. The cold head and the thermal path can be seen at the right. At the lower side, JADE-2 cards to control HAWAII-2RG arrays and SIDECAR ASICs are aligned.

Table 1. The lowest temperatures achieved during the 7th cooling test.

Position	Temperature
Cold Head	42.3K
Diaphragm	69.0K
Camera Lens Barrel (Blue Arm)	88.0K
Detector (Blue Arm)	87.5K
Camera Lens Barrel (Red Arm)	85.9K
Detector (Red Arm)	84.2K
Optical Bench	87.4K
Collimator	125.6K

cold-head of the GM-cycle cooler is connected. In addition to this thermal path, three more thermal paths are used to cool down the two detector cassettes and a molecular sieve unit (Figure 4)

4.2 Temperature during the 7th Cooling Test

Fully-assembled cooling test , where all the optical components including the collimator, camera lenses, dichroic mirror, detectors, filters, and grisms are installed, was been carried out in May 2016. This is the 7th cooling test of SWIMS at the laboratory, and its purpose is to carry out checkouts of focus adjustments which will be described in Section 5.2.

The cooling is assisted by a flow of liquid nitrogen (LN_2) through a precooling pipe installed at a cold frame inside the dewar. In total, 700 liter of LN_2 is consumed during the cool-down phase and the cryogenic components reached their minimum temperature in approximately 5 days.

Figure 5 shows the temperatures during the cool-down. The detector temperatures are kept higher than the other components using heaters, to avoid absorption of out-gas from the dewar jacket. The final temperature is summarized in Table 1, although there are slight fluctuations due to change in ambient temperature.

The final temperatures of the detector components are still higher than requirement of 80K, however, this is due to the thermal input from the camera lens barrels. We are now planning to isolate the detector cassettes thermally, and this will improve the detector temperatures below the requirement.

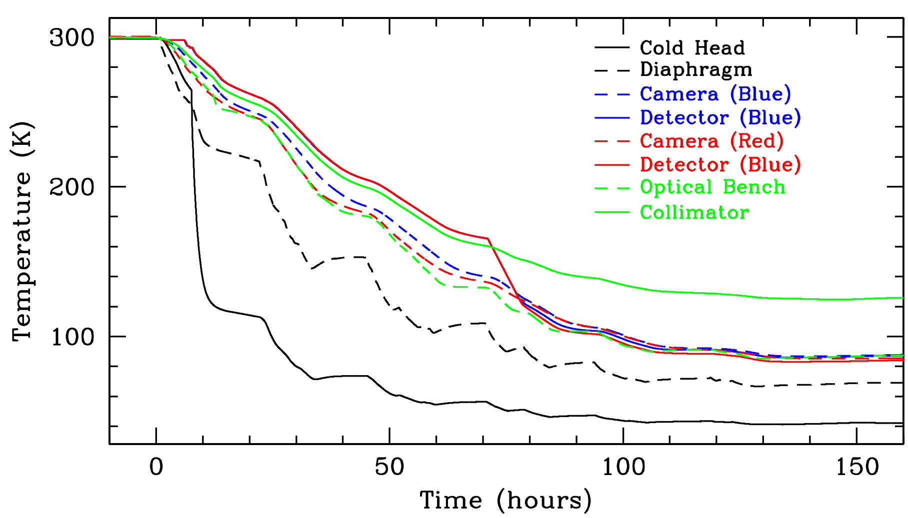

Figure 5. Temperature plot during the cooling test #7 in May 2016. The origin of the x-axis is set to time when the flow of LN_2 started, 2:00 of May 9 2016.

5. OPTICAL PERFORMANCE

5.1 Test Setup

The focal positions at the detector planes where the telescope focal plane is re-imaged, as well as image qualities of the optics, are evaluated using a special mask plate with pinholes, on the telescope focal plane in the MOSU dewar.

The mask plate has 25 pinholes on it, placed in five groups with five pinholes each. The five pinholes have different Z-axis (optical axis) offset from the telescope focal plane by -5mm, -2mm, 0mm, $+2$mm, and $+5$mm, which will be focused at the detector planes offset by $+830$ μm to -830μm. The diameter of the pinholes is 50μm, which corresponds to $\sim$1 pixel on the detector planes. Figure 6 shows this mask plate installed on the mask holder in the MOSU dewar, and the group of the five pinholes. The five groups of the pinholes are distributed within the focal plane to check the tilt of the detector surfaces.

5.2 Imaging Performance

The first image of the pinhole mask, which is the laboratory first light of SWIMS, is taken during the 6th cooling test on Dec. 15, 2015. In this image, pinholes with $+5$mm offset shows the smallest image size on the detector of $\sim$2 pixel in both the blue and the red arm. This suggests that the best focal positions are offset by $\sim -830\mu$m

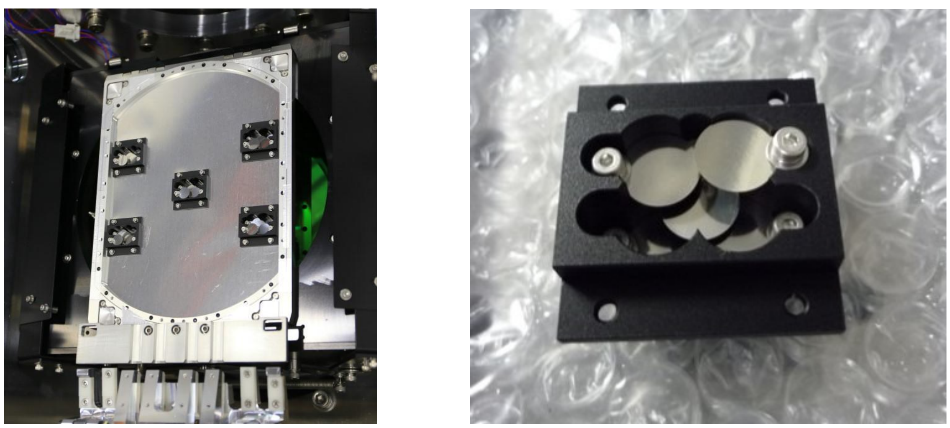

Figure 6. (Left) A pinhole mask installed on the mask holder, in front of the collimator lens. (Right) A group of pinholes, containing 5 pinholes offset by -5mm to $+5mm$ in z-axis.

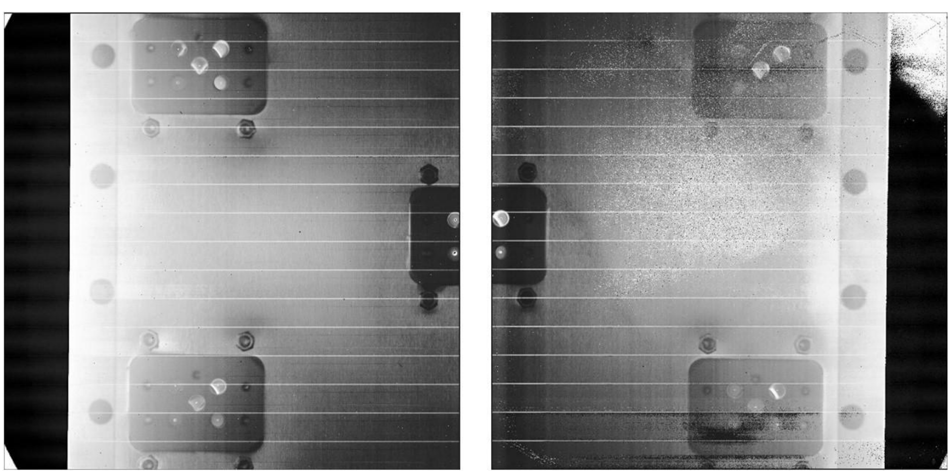

Figure 7. Pinhole mask images of the blue arm. Due to the degradation of one of the detectors, the right-hand side of the image is somewhat difficult to see, however, the five groups of the pinholes can be identified.

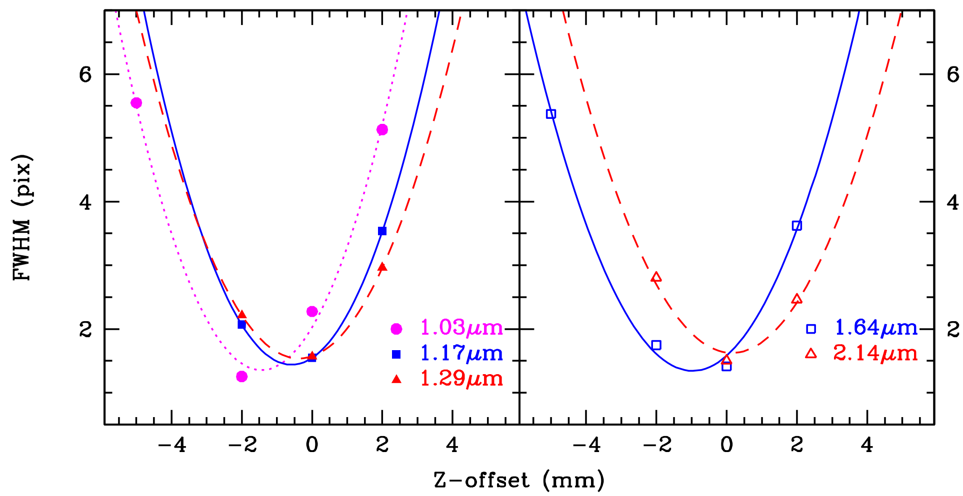

Figure 8. Image sizes of pinholes during the 7th cooling test, plotted against Z-axis offsets for the blue arm (left) and the red(right), measured at the temperature of 100K.

in the detector planes, probably because of the temperature of the lens barrels of $\sim$ 100K, which is higher than the design temperature of 65K.

To confirm how much focal shift will occur by temperature variation, we have carried out ray-trace simulations by

1. taking into account of thermal expansions of the optical bench and the lens barrels,
2. taking into account of thermal expansion of lens materials, and
3. modifying the refraction indices by interpolating the data point at 65K, 80K, and 293K[17]

and estimated focus offsets between 65K and 100K.

Then, the focal positions at the detector planes are estimated to shift by -0.92mm and -0.81mm for the blue and red arm, respectively, by changing the temperature from 65K to 100K, and the shift is consistent with the results of the 6th cooling test. Therefore, we have inserted a glass epoxy sheet of 0.6mm thick between the detector cassette and the camera lens barrel in each channel before we carry out the 7th cooling test mentioned in Section 4.2.

Figure 8 shows the offset of the pinholes along the Z-axis and image sizes for both arms, taken in the 7th cooling test at temperature of 100K. It can be seen that the smallest image sizes are obtained with the pinhole at $Z = 0$mm, and detectors are confirmed to be installed at the correct positions. The best image sizes are $\sim$ 1.5 pixels, and taking into account the intrinsic pinhole size of 1pixel, imaging quality of the optics is $\sim$ 1pixel, confirming that the optics has the performance as designed. No tilt of the detectors are found.

It can also be seen that wavelength dependencies of the best Z positions exist for both the blue and the red arms. The amount of the shift is maximum $\sim$ 1.5mm, and blurring caused by this offset is up to 2 pixels at 1.03μm. However, considering that typical slit width is 4 pixels ($0.''5$) and that the wavelength affected the most is at the shorter end of the blue channel, the effect of this chromatic aberration is very limited.

6. FLEXURE TEST

As SWIMS is installed on the Nasmyth focus of the TAO 6.5m telescope, where the instrument is overturned and rotated to compensate the field rotation, its stiffness against the change of the orientation is an important performance. To test this, we have carried out a flexure test by installing SWIMS on a telescope simulator at the laboratory in Japan (Figure 9). The simulator can change the orientation of the instruments by tilting its elevation axis and rotating its instrument rotator axis of the flange.

6.1 Configuration of the Work Surface in the Cryogenic Dewar

All the optical components of SWIMS is installed on the cold work surface as shown in Figure 2 and 9. This work surface is installed on the diaphragm as explained in Section 4.1, and the diaphragm is hung by the cold frame structure inside the dewar jacket. The cold frame is connected to the dewar jacket by three large blocks made of G-10 glass epoxy near the top lid of the dewar. We define the coordinates within the dewar as shown in the left panel of Figure 9, and use it throughout this section.

6.2 Displacement of the Slit Position

Displacement of the slit position against the flange center of a telescope, is difficult to measure as a slit mask is placed on the top of the collimator lens barrel which is kept at cryogenic temperature under vacuum environment.

We therefore measure the displacement of the collimator lens barrel against the wall of the MOSU dewar, assuming that the relative position between the telescope flange and the MOSU dewar is negligible The meaurement

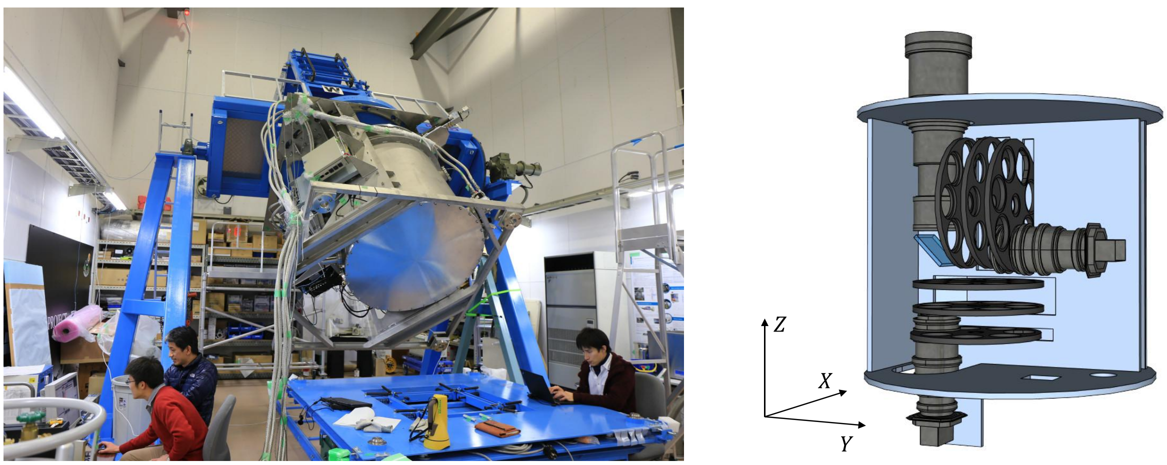

Figure 9. (Left) SWIMS under flexure test, installed on the telescope simulator. (Right) Coordinate system of SWIMS structure used in this paper.

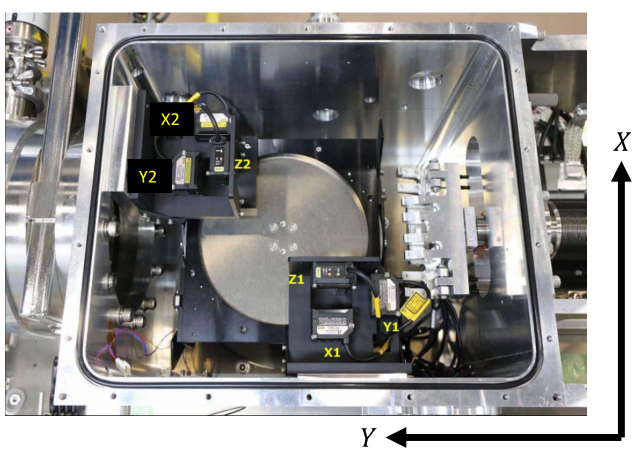

Figure 10. Configuration of the six laser displacement sensors in the MOSU dewar, whose layout is in two groups, each measuring the X, Y, and Z axis offsets.

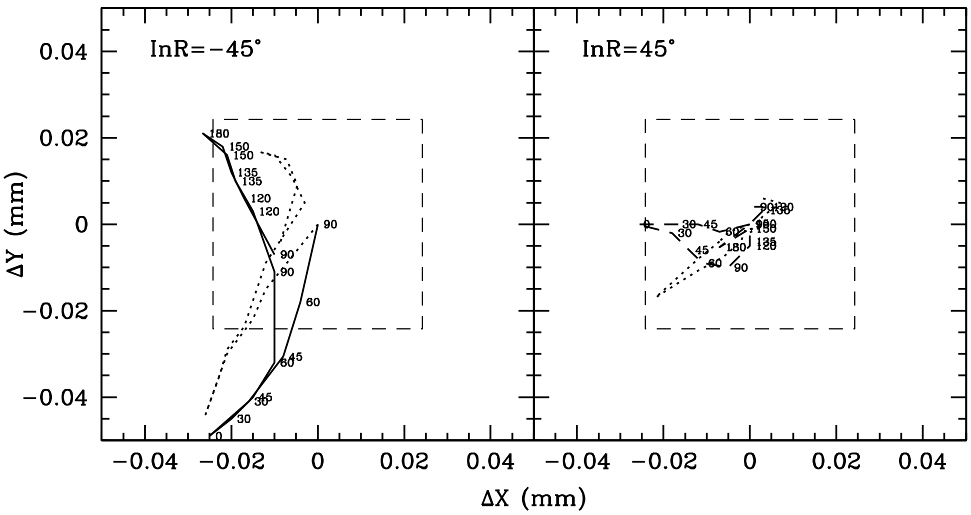

Figure 11. The results of the slit displacement test, tilted along the X-axis (left) and along the Y-axis (right). Rectangles with thin dashed line show the size of a pixel at the detector planes. Numbers in the plots show elevation angles in degree, where Z-axis pointing up at 90°.

is done by installing two targets of aluminum piece on the barrel and then measuring each X-Y-Z displacements by six laser displacement sensors. Figure 10 shows the configuration of the sensors, labeled by X1, Y1, Z1, X2, Y2, and Z2.

The displacement test was carried out during the 2nd cooling in November 2014. The dewar attached to the telescope simulator was tilted with fixed instrument rotator angle of InR= −45° and +45°. The elevation axis is the X-axis with InR= −45° and Y-axis with +45°. Figure 11 shows the result. It can be seen that the displacement is less than 2 pixel with elevation varied from 0° to 180°, fulfilling the requirements. Also the structure is found to be stiffer along the rotation of Y-axis than X-axis.

6.3 Displacement of the Detector Planes

Displacements of the detector planes against the telescope focal plane, that is, the position of slit masks, is measured by taking the pinhole images installed in the 6th cooling test. The measurements are carried out by first changing the elevation from El=90° to 1.5° with the instrument rotator angle fixed to InR= −48°, that is, tilted along the X-axis. Then, the instrument rotator is rotated by 360° with 90° intervals.

Figure 12 shows the result. The maximum displacement due to the InR angle is less than 2 pixels, and passes the requirement. The red arm has less stiffness compared to the blue arm, and shows offset of 2 pixels by tilting the whole optics by 90°.

7. SUMMARY AND FUTURE SCHEDULE

SWIMS is the first generation instrument for the TAO 6.5m infrared telescope, being constructed at the summit of Co. Chajnantor (5640m altitude), the world's highest observatory. Its development is now at the final stage, and we have confirmed its cryogenic, optical, and mechanical performances fulfilling the requirements.

Next, SWIMS is expected to be transported to the Subaru telescope in 2016 and planned to be installed on the Cassegrain focus of the telescope to carry out the first-light and engineering observations. After the completion of the 6.5m telescope, the collimator lens of SWIMS will be exchanged to that for the 6.5m telescope, as the optical parameters are different, and will be sent to Chile and SWIMS is expected to see the scientific first light in FY 2018.

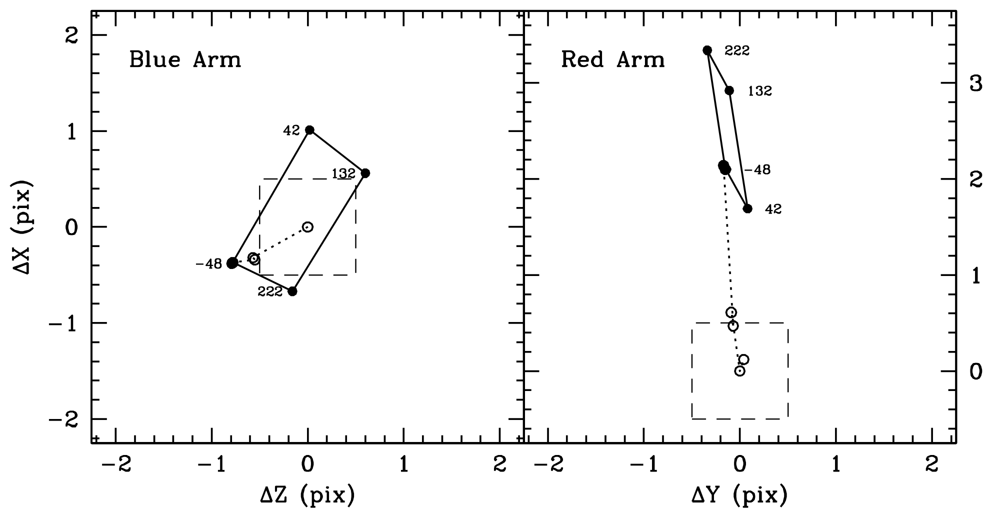

Figure 12. Offset positions of a pinhole at the detector planes during the flexure test. Rectangles with thin dashed line show the size of a pixel. The origin is the position of the pinhole with the elevation of 90°, where the cryostat of SWIMS is at the upright position. Open circles and dotted lines show trajectory of the pinhole with the elevation changed from 90° to 0°, fixing instrument rotator angle at InR= −48°. Filled circles and solid lines shows that with the instrument rotator angle changed by 360° fixing the elevation angle at El= 0°.

ACKNOWLEDGMENTS

This research is funded by a supplementary budget for economic stimulus packages formulated by Japanese government. Part of the development is supported by Ministry of Education, Culture, Sports, Science and Technology of Japan, Grant-in-Aid for Scientific Research (15H02062, 23540261, 24103003, 24244015, 2611460, and 266780) from the JSPS of Japan, and by the grant of Joint Development Research supported by the Research Coordination Committee, National Astronomical Observatory of Japan (NAOJ). The development activities are supported by the Advanced Technology Center, NAOJ.

REFERENCES

[1] Yoshii, Y., Doi, M., Kohno, K., Miyata, T., Motohara, K., Kawara, K., Tanaka, M., Minezaki, T., Sako, S., Morokuma, T., Tamura, Y., Tanabe, T., Takahashi, H., Konishi, M., Kamizuka, T., Kato, N., Aoki, T., Soyano, T., Tarusawa, K., Handa, T., Koshida, S., Bronfman, L., Ruiz, M. T., Hamuy, M., Mendez, R., and Garay, G., "The University of Tokyo Atacama Observatory 6.5m telescope: Project overview and current status," in [*Ground-based and Airborne Telescopes VI*], *Proc. SPIE*, in press (2016).

[2] Yoshii, Y., Doi, M., Kohno, K., Miyata, T., Motohara, K., Kawara, K., Tanaka, M., Minezaki, T., Sako, S., Morokuma, T., Tamura, Y., Tanabe, T., Takahashi, H., Konishi, M., Kamizuka, T., Koshida, S., Kato, N., Aoki, T., Soyano, T., Tarusawa, K., Handa, T., Bronfman, L., Ruiz, M. T., Hamuy, M., and Mendez, R., "Overview of University of Tokyo Atacama Observatory 6.5m telescope project," in [*Ground-based and Airborne Telescopes V*], *Proc. SPIE* **9145**, 914507 (2014).

[3] Yoshii, Y., Aoki, T., Doi, M., Handa, T., Kawara, K., Kato, D., Kohno, K., Konishi, M., Koshida, S., Minezaki, T., Mitani, N., Miyata, T., Motohara, K., Sako, S., Soyano, T., Tanabe, T., Tanaka, M., Tarusawa, K., Bronfman, L., Ruiz, M. T., and Hamuy, M., "The University of Tokyo Atacama Observatory 6.5m telescope project," in [*Ground-based and Airborne Telescopes III*], *Proc. SPIE* **7733**, 773308 (2010).

[4] Nakamura, T., Miyata, T., Sako, S., Asano, K., Uchiyama, M., Tanabe, T., Yoneda, M., Ita, Y., Onaka, T., Kataza, H., Aoki, T., Doi, M., Handa, T., Kato, D., Kawara, K., Kohno, K., Konishi, M., Koshida, S., Minezaki, T., Mitani, N., Motohara, K., Ohsawa, R., Soyano, T., Tanaka, M., Tarusawa, K., Toshikawa, K., and Yoshii, Y., "MiniTAO/MAX38 first light: 30-micron band observations from the ground-based

telescope," in [*Ground-based and Airborne Instrumentation for Astronomy III*], *Proc. SPIE* **7735**, 773561 (2010).

[5] Asano, K., Miyata, T., Sako, S., Kamizuka, T., Nakamura, T., Uchiyama, M., Yoneda, M., Kataza, H., Yoshii, Y., Doi, M., Kohno, K., Kawara, K., Tanaka, M., Motohara, K., Tanabe, T., Minezaki, T., Morokuma, T., Tamura, Y., Aoki, T., Soyano, T., Tarusawa, K., Kato, N., Konishi, M., Koshida, S., Takahashi, H., Handa, T., and Tateuchi, K., "Perfomance verification of the ground-based mid-infrared camera MAX38 on the MiniTAO Telescope," in [*Ground-based and Airborne Instrumentation for Astronomy IV*], *Proc. SPIE* **8446**, 844634 (2012).

[6] Tateuchi, K., Motohara, K., Konishi, M., Takahashi, H., Kato, N., Ohsawa, R., Yutaro, K., Yoshii, Y., Doi, M., Handa, T., Kohno, K., Kawara, K., Tanaka, M., Miyata, T., Minezaki, T., Sako, S., Tanabe, T., Morokuma, T., Tamura, Y., Aoki, T., Soyano, T., Tarusawa, K., Koshida, S., Kamizuka, T., Nakamura, T., Asano, K., and Uchiyama, M., "Development of a new calibration method for ground-based paschen-alpha imaging data," in [*Ground-based and Airborne Instrumentation for Astronomy IV*], *Proc. SPIE* **8446**, 84467D (2012).

[7] Tateuchi, K., Konishi, M., Motohara, K., Takahashi, H., Mitani Kato, N., Kitagawa, Y., Todo, S., Toshikawa, K., Sako, S., Uchimoto, Y. K., Ohsawa, R., Asano, K., Ita, Y., Kamizuka, T., Komugi, S., Koshida, S., Manabe, S., Nakamura, T., Nakashima, A., Okada, K., Takagi, T., Tanabé, T., Uchiyama, M., Aoki, T., Doi, M., Handa, T., Kawara, K., Kohno, K., Minezaki, T., Miyata, T., Morokuma, T., Soyano, T., Tamura, Y., Tanaka, M., Tarusawa, K., and Yoshii, Y., "Ground-based Paα Narrow-band Imaging of Local Luminous Infrared Galaxies. I. Star Formation Rates and Surface Densities," *The Astrophysical Journal Supplement Series* **217**, 1 (2015).

[8] Konishi, M., Motohara, K., Tateuchi, K., Takahashi, H., Kitagawa, Y., Kato, N., Sako, S., Uchimoto, Y. K., Toshikawa, K., Ohsawa, R., Yamamuro, T., Asano, K., Ita, Y., Kamizuka, T., Komugi, S., Koshida, S., Manabe, S., Matsunaga, N., Minezaki, T., Morokuma, T., Nakashima, A., Takagi, T., Tanabé, T., Uchiyama, M., Aoki, T., Doi, M., Handa, T., Kato, D., Kawara, K., Kohno, K., Miyata, T., Nakamura, T., Okada, K., Soyano, T., Tamura, Y., Tanaka, M., Tarusawa, K., and Yoshii, Y., "ANIR: Atacama near-infrared camera for the 1.0 m miniTAO telescope," *Publications of the Astronomical Society of Japan* **67**, 4 (2015).

[9] Konishi, M., Motohara, K., Takahashi, H., Tateuchi, K., Kitagawa, Y., Kato, N., Aoki, T., Doi, M., Handa, T., Kamizuka, T., Kawara, K., Kohno, K., Koshida, S., Minezaki, T., Miyata, T., Morokuma, T., Sako, S., Soyano, T., Tamura, Y., Tanabe, T., Tanaka, M., Tarusawa, K., and Yoshii, Y., "Design and development of SWIMS: a near-infrared multi-object spectrograph for the University of Tokyo Atacama Observatory," in [*Ground-based and Airborne Instrumentation for Astronomy IV*], *Proc. SPIE* **8446**, 84467P (2012).

[10] Motohara, K., Konishi, M., Takahashi, H., Tateuchi, K., Kitagawa, Y., Todo, S., Kato, N. M., Ohsawa, R., Aoki, T., Asano, K., Doi, M., Kamizuka, T., Kawara, K., Kohno, K., Koshida, S., Minezaki, T., Miyata, T., Morokuma, T., Okada, K., Sako, S., Soyano, T., Tamura, Y., Tanabe, T., Tanaka, M., Tarusawa, K., Uchiyama, M., and Yoshii, Y., "Development of a simultaneous two-color near-infrared multi-object spectrograph SWIMS for the TAO 6.5-m telescope," in [*Ground-based and Airborne Instrumentation for Astronomy V*], *Proc. SPIE* **9147**, 91476K (2014).

[11] Takahashi, H., Konishi, M., Motohara, K., Kato, N. M., Tateuchi, K., Kitagawa, Y., and Todo, S., "Development of multi-object spectroscopy unit for simultaneous-color wide-field infrared multi-object spectrograph," in [*Ground-based and Airborne Instrumentation for Astronomy V*], *Proc. SPIE* **9147**, 91476N (2014).

[12] Kitagawa, Y., Ozaki, S., Motohara, K., Konishi, M., Takahashi, H., Tateuchi, K., Todo, S., Kato, N., and Yoshikawa, T., "Fabrication of a wide-field NIR integral field unit for SWIMS using ultra-precision cutting," in [*Advances in Optical and Mechanical Technologies for Telescopes and Instrumentation*], *Proc. SPIE*, in press (2016).

[13] Kitagawa, Y., Ozaki, S., Motohara, K., Konishi, M., Takahashi, H., Tateuchi, K., Todo, S., Kato, N., and Yoshikawa, T., "Concept and optical design of the near-infrared integral field unit for SWIMS," in [*Advances in Optical and Mechanical Technologies for Telescopes and Instrumentation*], *Proc. SPIE* **9151**, 91514P (2014).

[14] Ozaki, S., Kitagawa, Y., Motohara, K., Konishi, M., Takahashi, H., Yoshikawa, T., Tateuchi, K., and Kato, N., "Development of an integral field unit for a near-infrared multi-object imaging spectrograph SWIMS,"

in [*Modern Technologies in Space- and Ground-based Telescopes and Instrumentation II*], *Proc. SPIE* **8450**, 84503Y (2012).

[15] Terao, Y., Motohara, K., Konishi, M., Takahashi, H., Kato, N., Kitagawa, Y., Kobayakawa, Y., Ohashi, H., Tateuchi, K., and Todo, S., "NIR camera and spectrograph SWIMS for TAO 6.5m telescope: array control system and its performance," in [*High Energy, Optical, and Infrared Detectors for Astronomy VII*], *Proc. SPIE*, in press (2016).

[16] Jeschke, E. and Inagaki, T., "Lessons learned deploying a second generation Observation Control System for Subaru Telescope," in [*Software and Cyberinfrastructure for Astronomy*], *Society of Photo-Optical Instrumentation Engineers (SPIE) Conference Series* **7740**, 77400F (2010).

[17] Yamamuro, T., Sato, S., Zenno, T., Takeyama, N., Matsuhara, H., Maeda, I., and Matsueda, Y., "Measurement of refractive indices of 20 optical materials at low temperatures," *Optical Engineering* **45**, 083401 (2006).

NIR camera and spectrograph SWIMS for TAO 6.5m telescope: array control system and its performance

Yasunori Terao[a], Kentaro Motohara[a], Masahiro Konishi[a], Hidenori Takahashi[a], Natsuko M. Kato[a], Yutaro Kitagawa[a], Yutaka Kobayakawa[a], Hirofumi Ohashi[a], Ken Tateuchi[a], and Soya Todo[a]

[a]Institute of Astronomy, Graduate School of Science, The University of Tokyo, 2-21-1 Osawa, Mitaka Tokyo 181-0015, Japan

ABSTRACT

SWIMS (Simultaneous-color Wide-field Infrared Multi-object Spectrograph) is a near-infrared imager and multi-object spectrograph as one of the first generation instruments for the University of Tokyo Atacama Observatory (TAO) 6.5m telescope. In this paper, we describe an array control system of SWIMS and results of detector noise performance evaluation. SWIMS incorporates four (and eight in future) HAWAII-2RG focal plane arrays for detectors, each driven by readout electronics components: a SIDECAR ASIC and a JADE2 Card. The readout components are controlled by a HAWAII-2RG Testing Software running on a virtual Windows machine on a Linux PC called array control PC. All of those array control PCs are then supervised by a SWIMS control PC. We have developed an "array control software system", which runs on the array control PC to control the HAWAII-2RG Testing Software, and consists of a socket client and a dedicated server called device manager. The client runs on the SWIMS control PC, and the device manager runs on the array control PC. An exposure command, issued by the client on the SWIMS control PC, is sent to the multiple device managers on the array control PCs, and then multiple HAWAII-2RGs are driven simultaneously. Using this system, we evaluate readout noise performances of the detectors, both in a test dewar and in a SWIMS main dewar. In the test dewar, we confirm the readout noise to be 4.3 e^- r.m.s. by 32 times multiple sampling when we operate only a single HAWAII-2RG, whereas in the case of simultaneous driving of two HAWAII-2RGs, we still obtain sufficiently low readout noise of ~ 10 e^- r.m.s.. In the SWIMS main dewar, although there are some differences between the detectors, the readout noise is measured to be 4.1–4.6 e^- r.m.s. with simultaneous driving by 64 times multiple sampling, which meets the requirement for background-limited observations in J band of ~ 14 e^- r.m.s..

Keywords: HAWAII-2RG, SWIMS, near-infrared, TAO

1. INTRODUCTION

We are developing a near-infrared camera and spectrograph SWIMS (Simultaneous-color Wide-field Infrared Multi-object Spectrograph)[1–3] as a first-generation near-infrared instrument for the University of Tokyo Atacama Observatory (TAO, P.I.: Yuzuru Yoshii)[4–6] 6.5m infrared telescope which is now under construction at the world's highest astronomical site, the summit of Cerro Chajnantor (an altitude of 5,640 m or 18,500 ft) in northern Chile. SWIMS has capabilities of wide-field ($\phi 9.6'$) two-color simultaneous imaging and MOS (Multi-Object Spectroscopy) across the entire NIR wavelength range by splitting incident light into blue (0.9–1.4 μm) and red (1.4–2.5 μm) arms using a dichroic mirror . Therefore, SWIMS has two focal planes and each of them is covered by two HAWAII-2RG (HgCdTe Astronomy Wide Area Infrared Imager with 2K $\times$ 2K resolution, Reference pixels and Guide mode; 2.5 μm cutoff)[7] detectors.

In this paper, we introduce array control system of SWIMS and show results of detector performance tests using this system. In Section 2 and 3 we overview the hardware and software of the array system. In Section 4, we present readout noise performance of our system, and in Section 5 we summarize them.

Further author information: (Send correspondence to Y.T.)
Y.T. : E-mail: y_terao@ioa.s.u-tokyo.ac.jp

High Energy, Optical, and Infrared Detectors for Astronomy VII, edited by Andrew D. Holland, James Beletic, Proc. of SPIE Vol. 9915, 99151W · © 2016 SPIE · CCC code: 0277-786X/16/$18 · doi: 10.1117/12.2232014

2. HARDWARE OF ARRAY SYSTEM

SWIMS has four (eight in future) HAWAII-2RGs and both the blue and red arms have two of them each (Figure 1). The detectors are driven by SIDECAR ASICs and JADE2 Cards. The SIDECAR ASICs generate clocks for driving the HAWAII-2RGs, amplify output signals and perform A/D conversion. The JADE2 Cards supply the SIDECAR ASICs with power and communication with control software. Each HAWAII-2RG is driven by a pair of the SIDECAR ASIC and the JADE2 Card.

One of the features of the HAWAII-2RGs is existence of reference pixels. The reference pixels do not have photodiodes to detect infrared photons and are located outside of normal pixels with width of 4 pixels. They have same circuit for readout as the normal pixels, and are useful to measure readout noises and to correct bias level fluctuations.

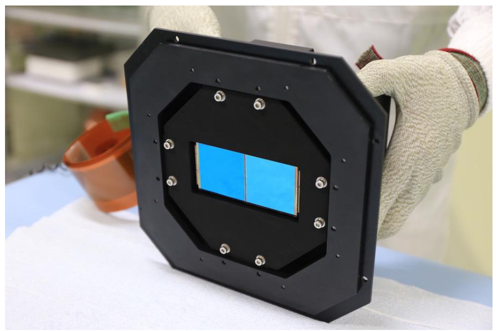

Figure 1. Two HAWAII-2RGs mounted on a detector cassette.

Figure 2 shows an overview of hardware of the SWIMS array system. The HAWAII-2RGs and the SIDECAR ASICs for each arm are installed into a detector cassette and attached to a camera-lens barrel installed on an optical bench which is kept under cryogenic temperature (~ 80 K) in vacuum environment. The JADE2 Cards are installed on an inner wall of the dewar jacket, under room temperature in vacuum environment (Figure 3). The SIDECAR ASICs and the JADE2 Cards are connected by flat cables through which clock patterns and A/D converted signals are sent, as well as powers to the SIDECAR ASICs are supplied. As distance between the JADE2 Cards and the SIDECAR ASICs are large, we have manufactured long flat cables having length of 1.7 m. Two types of flat cables are manufactured, one is that without shield, and the other with shield. Figure 4 shows the flat cable with the shield. The JADE2 Cards are then connected with array control PCs located outside of the SWIMS main dewar through USB 2.0 interface to communicate with softwares for driving the detectors. Each array system on the blue or red arm has the array control PC to control them. The array control PCs are then controlled by a SWIMS control PC.

3. ARRAY CONTROL SOFTWARE SYSTEM

As the control software of the JADE2 Cards, called the HAWAII-2RG Testing Software provided by Teledyne Imaging Sensors, only runs on Windows OS, we have constructed array control software system to handle the Testing Software running in virtual Windows machines running in the Linux OS on the array control PC. Figure 5 shows an overview of the array control software system. The system consists of three components, a client on the SWIMS control PC, a device manager on the array control PC, and HAWAII-2RG Testing Softwares on the virtual Windows machines in the array control PC. The client communicates with the device manager by server-and-client communication. The device manager is composed of two parts, one is a server to communicate with the clients, and the other is to communicate with the HAWAII-2RG Testing Softwares. A command issued from the client is arranged and sent to the Testing Softwares by the device managers using socket communication. The client and the device manager of the array control software system are scripted by Python. Using Python threading module, commands can be issued from the clients to the device managers even when a previous command is still being processed.

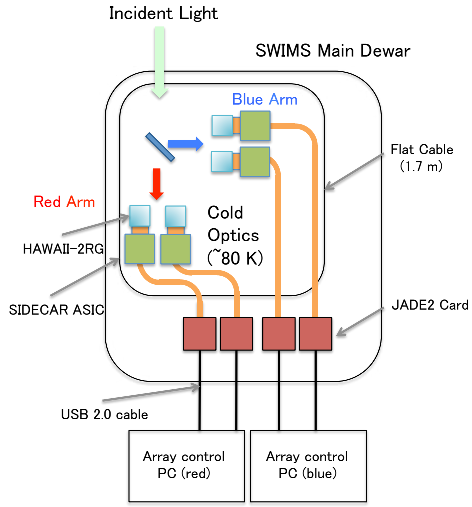

Figure 2. Internal layout of arrat system in the SWIMS dewar. HAWAII-2RGs and SIDECAR ASICs are in cold optics and kept under cryogenic temperature (~ 80 K) in vacuum environment. JADE2 Cards are used under room temperature in vacuum environment.

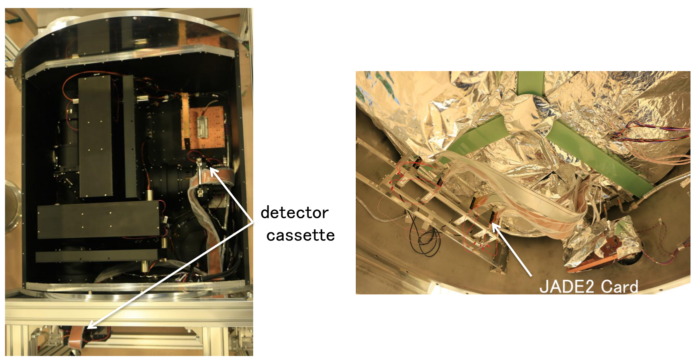

Figure 3. (Left) The optical bench of SWIMS. The HAWAII-2RGs and the SIDECAR ASICs are mounted on the detector cassettes indicated by arrows. (Right) Location of the JADE2 Cards, which are installed in a rack attached to the inner wall of the dewar jacket.

Status information such as detector temperature, configuration parameters and frame ID is stored in Relational DataBase Management System (RDBMS) on the SWIMS control PC. The device managers get the status information before, after, and during an exposure, and save them to headers of produced FITS files.

Commands from the client software are almost simultaneously sent to HAWAII-2RG Testing Softwares via servers. However, we find that there are typically ~ 1 second differences between time stamps of two acquired files when we drive two HAWAII-2RGs simultaneously. Figure 6 shows distributions of the time differences. There is a peak around 1 sec and only 17% of data pairs have time difference less than 1 sec. This result suggests that there is a time difference between clock sent to two detectors, and thus this differences may be a cause of noise patterns which appear in acquired images when we drive multiple HAWAII-2RGs simultaneously (see Section 4.3.2).

4. READOUT NOISE PERFORMANCE

We have carried out tests to evaluate readout noise performances of HAWAII-2RGs, both in a test dewar and the SWIMS main dewar.

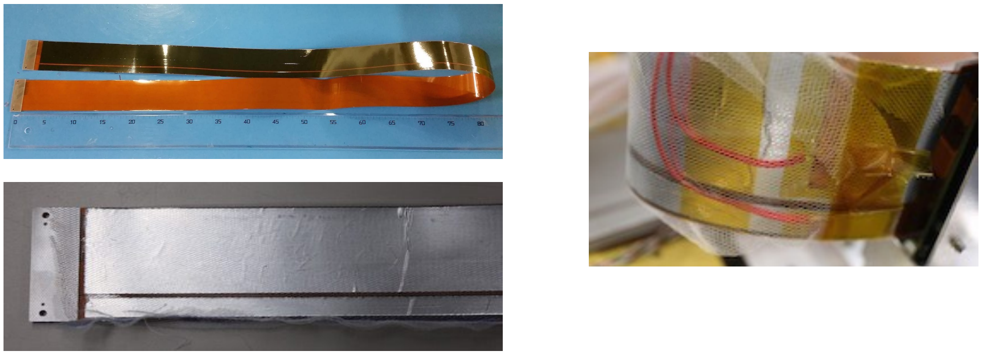

Figure 4. (Upper left) The flat cable with a shield, before adhering aluminum tapes on the non-shield side. The dark layers seen on the upper side of the cable is the internal shield layer. (Lower left) The other side of the cable is covered by aluminum tapes. (Right) Copper wires are soldered to the shields to ground them to the dewar.

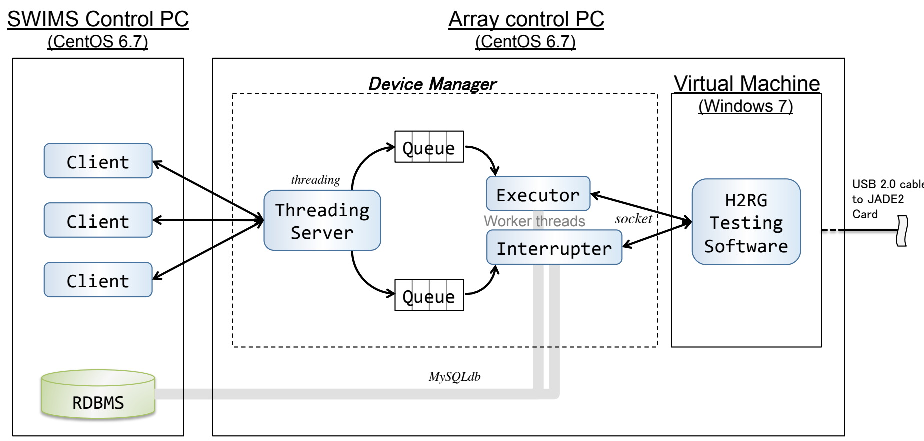

Figure 5. An overview of the array control software system. Two Windows virtual machines run on the Linux OS of the array control PC of each arms to drive the two HAWAII-2RGs each.

4.1 Method of Measurements

Measurements of readout noise are carried out in the following manner. First, we make a difference image from two correlated double sampling (CDS) images which are obtained under a dark condition with shortest integration time of 1.48 sec. We then divide the difference image by $\sqrt{2}$ and calculate standard deviation of pixel counts, which have a unit of Analog-to-Digital Unit (ADU). Multiplying the standard deviation by conversion factor g_c [e^-/ADU], we finally get an estimate of the readout noise $\sigma_{\rm read}$.

We also carried out multiple sampling, which performs $n_{\rm read}$ times readout before and after an exposure. Each $n_{\rm read}$ images are averaged to create a CDS image by subtracting two average images each other.[8] Ideally readout noise decreases with $\sigma_{\rm read} \propto n_{\rm read}^{-0.5}$ by this method. $n_{\rm read} = 1$ corresponds to a normal CDS.

4.2 Performance in the Test Dewar

4.2.1 Test Setup

Figure 7 shows the setup in the test dewar. The two HAWAII-2RGs are mounted on the detector cassette and cooled down to 80 K. The JADE2 Cards are mounted on a rack inside the dewar under room temperature and vacuum condition. In this way, we make similar environment to the SWIMS main dewar and drive the two HAWAII-2RGs simultaneously.

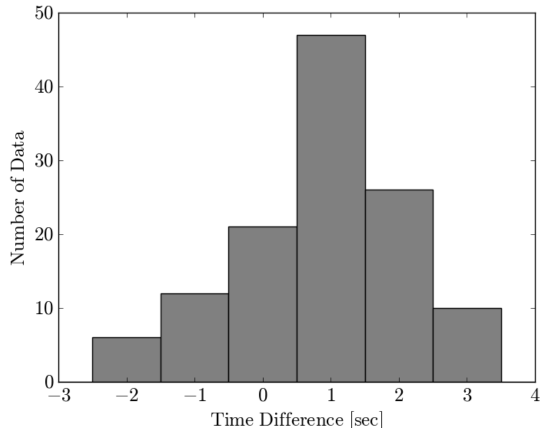

Figure 6. A distribution of differences between time stamps saved in the FITS headers of two acquired data which are obtained by same timing commands.

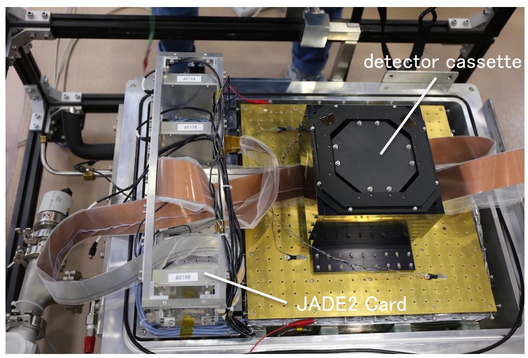

Figure 7. An experimental setup of the test dewar. The two HAWAII-2RGs and the SIDECAR ASICs are mounted on a black detector cassette. The SIDECAR ASICs are connected to the JADE2 Cards mounted on the rack by the flat cables.

We adopt a slow readout mode which has pixel rate of 100 kHz and a 32 channel output mode, under which it takes ~ 1.48 seconds to readout a single frame. Preamp gain is set to 5.66, and consequently we get a conversion factor of $g_c \sim 2.28\ e^-$/ADU in a manner described in Todo et al. (2012).[9]

4.2.2 Results

First, we drive the two HAWAII-2RGs simultaneously using the flat cables without shield, and find that when $n_{\rm read} = 1$, readout noise of simultaneous driving is $\sim 92\ e^-$ r.m.s., nearly four times larger than that of single driving of $\sim 24\ e^-$ r.m.s.. We also find short-cycle (~ 5 Hz) noise patterns and scratch patterns in images of simultaneous driving as shown in Figure 8.

We next carry out the same measurement with the flat cables with shield (Figure 8). Although the short-cycle noise patterns disappear and the readout noise of simultaneous driving decrease to $\sim 33\ e^-$ r.m.s., the scratch patterns with black or white vertical lines remain in images (also see section 4.3.2). The requirement for the readout noise is less than $\sim 14\ e^-$ r.m.s. to perform background limited observations in J band even without OH airglow, and our results of both single and simultaneous drivings do not meet it. However, using the multiple sampling method, the readout noise decreases and we find that it is minimized with $n_{\rm read} = 32$ to $4.3\ e^-$ r.m.s. for the single driving, and to $\sim 10\ e^-$ r.m.s. for the simultaneous driving. Therefore, we confirm that the requirement for the readout noise is met using the multiple sampling method.

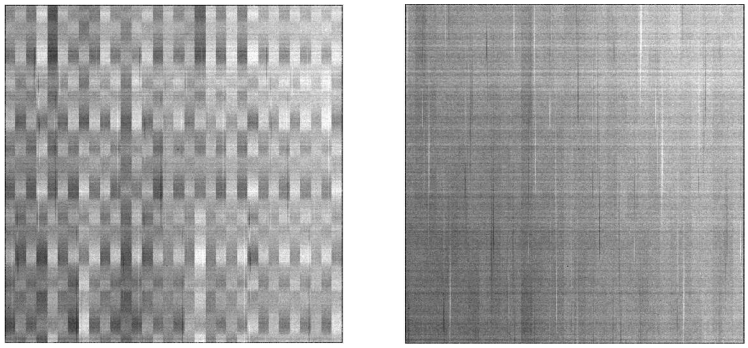

Figure 8. CDS images obtained under dark conditions with integration time of 1.48 sec using the flat cables without shield (left) and with shield (right) in the test dewar.

4.3 Performance in the SWIMS Main Dewar

4.3.1 Test Setup

We install the all four HAWAII-2RGs in the SWIMS main dewar and perform readout noise tests by driving a single detector (single driving), two detectors simultaneously (double driving), and four detectors simultaneously (quadruple driving). Because the detector temperatures are high ($\sim$ 110 K) due to high heat input from uncorrectly-set large stop currents of filter wheels, dark current levels are too high to measure the readout noise in full frames. Therefore, we measure the readout noise by only using the reference pixels. In addition, since one of the detectors, HAWAII-2RG #208, suffers from degradation, we only show results of the other three detectors.

Almost all configurations are same as those for the test dewar except for reference and bias voltages. We adjusted them to set the bias count of each HAWAII-2RGs to be at the same level.[10]

4.3.2 Results

The results are shown in Table 1. Figure 9 shows the readout noise with increasing $n_{\rm read}$ from 1 to 64. In this range, the readout noise continue to decrease nearly following $\sigma_{\rm read} \propto n_{\rm read}^{-0.5}$. Although there are slight differences between the three HAWAII-2RGs, the readout noises decrease from 18.6–25.9 e^- r.m.s. with $n_{\rm read} = 1$ to 3.3–4.3 e^- r.m.s. with $n_{\rm read} = 64$ in the single driving. Even in the multiple driving (that is, double or quadruple driving), the readout noises decrease from 21.3–29.3 e^- r.m.s. with $n_{\rm read} = 1$ to 4.1–4.6 e^- r.m.s. with $n_{\rm read} = 64$, and there is no significant difference between double and quadruple drivings. Therefore, we conclude that the readout noise performances meet the SWIMS requirement ($\sigma_{\rm read} \lesssim 14$ e^- r.m.s.) in the main dewar using the multiple sampling method.

Comparing CDS images of the single and the multiple drivings, there are again vertical scratch patterns in images of the multiple driving just like the images of the test dewar experiment (Figure 10). By changing the configurations, we find that these lines seem to be caused by differences of reset timings between the detectors. Resets of the detectors are performed continuously during their idle state and just before their first readout of integrations. In the multiple drivings, they will be performed at slightly different timings in different detectors, which arises from the difference of the command execution timings between each HAWAII-2RGs Testing Softwares mentioned in Section 3.

5. SUMMARY

We develop the array control system of the near-infrared camera and spectrograph for the TAO 6.5m telescope, SWIMS. The software system runs on the Linux PCs to control the HAWAII-2RG Testing Software in the virtual Windows machines, and consists of clients and device managers. By using server and client communication between the client on the SWIMS control PC and the device managers on the array control PC, and socket communication between the device managers and the HAWAII-2RG Testing Softwares, we can drive all HAWAII-2RGs simultaneously.

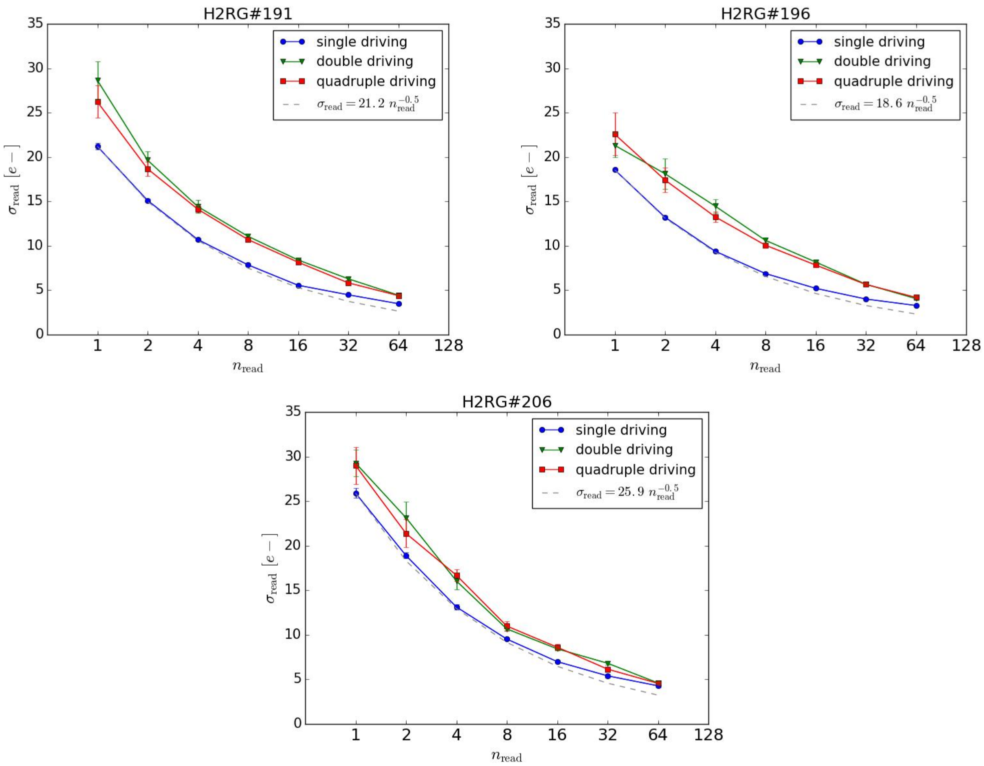

Figure 9. Readout noises of multiple sampling measured by using only reference pixels. Blue, green, and red solid lines show readout noise of single, double, and quadruple drivings. Gray dashed curves show the relation of $\sigma_{\rm read} = \sigma_0 n_{\rm read}^{-0.5}$. σ_0 is the noise of single drivings with $n_{\rm read} = 1$.

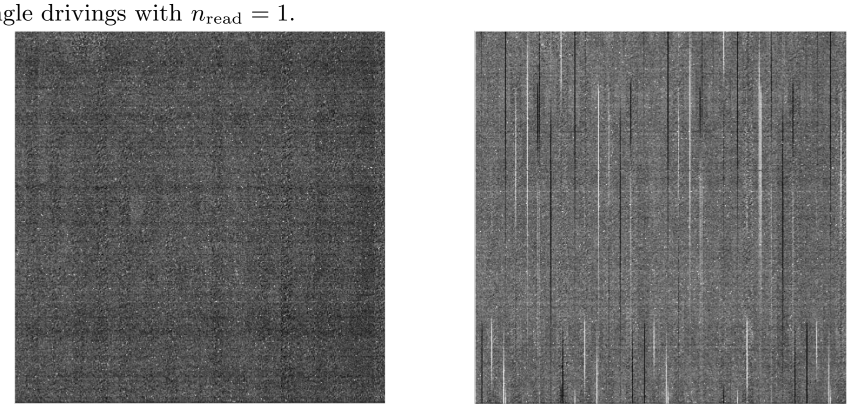

Figure 10. CDS images of single (left panel) or multiple (right panel) drivings obtained under dark conditions and exposure time of 1.48 sec in the SWIMS dewar.

We next evaluate the performances using this system, both in the test dewar and the SWIMS main dewar. In test dewar, we find that the readout noise of simultaneous driving decrease from $\sim 33\ e^-$ r.m.s. to $4.3\ e^-$ r.m.s. by 32 times multiple sampling. Even in test SWIMS main dewar, we confirm that the readout noise decrease from 21.3–29.3 e^- r.m.s. to 4.1–4.6 e^- r.m.s. by 64 times multiple sampling in double driving and quadruple driving. Therefore, we can achieve SWIMS requirement of $\sigma_{\rm read} \lesssim 14\ e^-$ r.m.s. even in simultaneous driving of multiple HAWAII-2RGs.

The short-cycle noise patterns in images of simultaneous driving disappear by using the flat cables with shield. However, the scratch patterns still remain. We find that they are possibly related to the differences of reset timings of the detectors, and it may be cancelled by synchronizing start timings of exposures.

Table 1. Results of readout noise measurements with $n_{\mathrm{read}} = 1$–64 at the SWIMS main dewar. Note that these readout noise are measured using reference pixels to avoid influences of high dark currents.

HAWAII-2RG		#191			#196			#206		
SIDECAR ASIC		#46			#54			#52		
# of driving HAWAII-2RGs		1	2	4	1	2	4	1	2	4
Readout Noise with various n_{read} (e^- r.m.s.)	1	21.2	28.6	26.2	18.6	21.3	22.6	25.9	29.3	29.0
	2	15.1	19.7	18.7	13.2	18.1	17.4	18.9	23.1	21.4
	4	10.7	14.4	14.1	9.4	14.5	13.3	13.1	16.1	16.7
	8	7.9	11.1	10.7	6.9	10.6	10.1	9.5	10.7	11.0
	16	5.6	8.4	8.2	5.2	8.2	7.8	7.0	8.4	8.6
	32	4.5	6.3	5.8	4.0	5.7	5.7	5.4	6.8	6.2
	64	3.5	4.4	4.4	3.3	4.1	4.2	4.3	4.6	4.6

ACKNOWLEDGMENTS

Development of SWIMS is funded by a supplementary budget for economic stimulus packages formulated by Japanese government. Part of this research is supported by Ministry of Education, Culture, Sports, Science and Technology of Japan, Grant-in-Aid for Scientific Research (15H02062, 23540261, 24103003, 24244015, 2611460, and 266780) from the JSPS of Japan, and by the grant of Joint Development Research supported by the Research Coordination Committee, National Astronomical Observatory of Japan (NAOJ). The development activities of SWIMS are supported by the Advanced Technology Center, NAOJ.

REFERENCES

[1] Motohara, K., Konishi, M., Takahashi, H., Kato, N. M., Kitagawa, Y., Kobayakawa, Y., Terao, Y., Ohashi, H., Aoki, T., Doi, M., Kamizuka, T., Kohno, K., Minezaki, T., Miyata, T., Morokuma, T., Mori, K., Ohsawa, R., Okada, K., Sako, S., Soyano, T., Tamura, Y., Tanabe, T., Tanaka, M., Tarusawa, K., Uchiyama, M., Koshida, S., Asano, K., Tateuchi, K., Uchiyama, M., Todo, S., and Yoshii, Y., "NIR camera and spectrograph SWIMS for TAO 6.5m telescope : Overview and development status," in [*Ground-based and Airborne Instrumentation for Astronomy VI*], *Proc. SPIE*, in press (2016).

[2] Motohara, K., Konishi, M., Takahashi, H., Tateuchi, K., Kitagawa, Y., Todo, S., Kato, N. M., Ohsawa, R., Aoki, T., Asano, K., Doi, M., Kamizuka, T., Kawara, K., Kohno, K., Koshida, S., Minezaki, T., Miyata, T., Morokuma, T., Okada, K., Sako, S., Soyano, T., Tamura, Y., Tanabe, T., Tanaka, M., Tarusawa, K., Uchiyama, M., and Yoshii, Y., "Development of a simultaneous two-color near-infrared multi-object spectrograph SWIMS for the TAO 6.5-m telescope," in [*Ground-based and Airborne Instrumentation for Astronomy V*], *Proc. SPIE* **9147**, 91476K (2014).

[3] Konishi, M., Motohara, K., Takahashi, H., Tateuchi, K., Kitagawa, Y., Kato, N., Aoki, T., Doi, M., Handa, T., Kamizuka, T., Kawara, K., Kohno, K., Koshida, S., Minezaki, T., Miyata, T., Morokuma, T., Sako, S., Soyano, T., Tamura, Y., Tanabe, T., Tanaka, M., Tarusawa, K., and Yoshii, Y., "Design and development of SWIMS: a near-infrared multi-object spectrograph for the University of Tokyo Atacama Observatory," in [*Ground-based and Airborne Instrumentation for Astronomy IV*], *Proc. SPIE* **8446**, 84467P (2012).

[4] Yoshii, Y., Doi, M., Kohno, K., Miyata, T., Motohara, K., Kawara, K., Tanaka, M., Minezaki, T., Sako, S., Morokuma, T., Tamura, Y., Tanabe, T., Takahashi, H., Konishi, M., Kamizuka, T., Kato, N., Aoki, T., Soyano, T., Tarusawa, K., Handa, T., Koshida, S., Bronfman, L., Ruiz, M. T., Hamuy, M., Mendez, R., and Garay, G., "The University of Tokyo Atacama Observatory 6.5m telescope: Project overview and current status," in [*Ground-based and Airborne Telescopes VI*], *Proc. SPIE*, in press (2016).

[5] Yoshii, Y., Doi, M., Kohno, K., Miyata, T., Motohara, K., Kawara, K., Tanaka, M., Minezaki, T., Sako, S., Morokuma, T., Tamura, Y., Tanabe, T., Takahashi, H., Konishi, M., Kamizuka, T., Koshida, S., Kato, N., Aoki, T., Soyano, T., Tarusawa, K., Handa, T., Bronfman, L., Ruiz, M. T., Hamuy, M., and Mendez,

R., "Overview of University of Tokyo Atacama Observatory 6.5m telescope project," in [*Ground-based and Airborne Telescopes V*], *Proc. SPIE* **9145**, 914507 (2014).

[6] Yoshii, Y., Aoki, T., Doi, M., Handa, T., Kawara, K., Kato, D., Kohno, K., Konishi, M., Koshida, S., Minezaki, T., Mitani, N., Miyata, T., Motohara, K., Sako, S., Soyano, T., Tanabe, T., Tanaka, M., Tarusawa, K., Bronfman, L., Ruiz, M. T., and Hamuy, M., "The University of Tokyo Atacama Observatory 6.5m telescope project," in [*Ground-based and Airborne Telescopes III*], *Proc. SPIE* **7733**, 773308 (2010).

[7] Beletic, J. W., Blank, R., Gulbransen, D., Lee, D., Loose, M., Piquette, E. C., Sprafke, T., Tennant, W. E., Zandian, M., and Zino, J., "Teledyne Imaging Sensors: infrared imaging technologies for astronomy and civil space," in [*High Energy, Optical, and Infrared Detectors for Astronomy III*], *Proc. SPIE* **7021**, 70210H (2008).

[8] Fowler, A. M. and Gatley, I., "Demonstration of an algorithm for read-noise reduction in infrared arrays," *ApJ* **353**, L33 (1990).

[9] Todo, S., Tateuchi, K., Motohara, K., Konishi, M., Takahashi, H., Kitagawa, Y., and Kato, N. M., "Optimization and performance of H2RG detectors and SIDECAR ASICs for SWIMS," in [*High Energy, Optical, and Infrared Detectors for Astronomy VI*], *Proc. SPIE* **9154**, 91541L (2014).

[10] Crouzet, P.-E., ter Haar, J., de Wit, F., Beaufort, T., Butler, B., Smit, H., van der Luijt, C., and Martin, D., "Characterization of HAWAII-2RG detector and SIDECAR ASIC for the Euclid mission at ESA," in [*High Energy, Optical, and Infrared Detectors for Astronomy V*], *Proc. SPIE* **8453**, 84531R (2012).

Fabrication of a wide–field NIR integral field unit for SWIMS using ultra–precision cutting

Yutaro Kitagawa[a], Yutaka Yamagata[b], Shin-ya Morita[b,c], Kentaro Motohara[a], Shinobu Ozaki[d], Hidenori Takahashi[a], Masahiro Konishi[a], Natsuko M. Kato[a], Yutaka Kobayakawa[a], Yasunori Terao[a], and Hirofumi Ohashi[a]

[a]Institute of Astronomy, Graduate School of Science, The University of Tokyo, 2-21-1 Osawa, Mitaka, Tokyo 181-0015, Japan

[b]RIKEN Center for Advanced Photonics (RAP), RIKEN, 2-1 Hirosawa, Wako, Saitama 351-0198, Japan

[c]Faculty of Engineering, Tokyo Denki University, 5 Senju Asahi-cho, Adachi-ku, Tokyo 120-8551, Japan

[d]National Astronomical Observatory of Japan, 2-21-1 Osawa, Mitaka, Tokyo 181-8588, Japan

ABSTRACT

We describe overview of fabrication methods and measurement results of test fabrications of optical surfaces for an integral field unit (IFU) for Simultaneous–color Wide–field Infrared Multi–object Spectrograph, SWIMS, which is a first–generation instrument for the University of Tokyo Atacama Observatory 6.5-m telescope. SWIMS–IFU provides entire near-infrared spectrum from 0.9 to 2.5 μm simultaneously covering wider field of view of $17'' \times 13''$ compared with current near–infrared IFUs. We investigate an ultra–precision cutting technique to monolithically fabricate optical surfaces of IFU optics such as an image slicer. Using 4– or 5–axis ultra precision machine we compare the milling process and shaper cutting process to find the best way of fabrication of image slicers. The measurement results show that the surface roughness almost satisfies our requirement in both of two methods. Moreover, we also obtain ideal surface form in the shaper cutting process. This method will be adopted to other mirror arrays (*i.e.* pupil mirror and slit mirror, and such monolithic fabrications will also help us to considerably reduce alignment procedure of each optical elements.

Keywords: integral field unit, ultra-precision cutting, TAO 6.5–m telescope, , near–infrared

1. INTRODUCTION

Recently integral field spectroscopy (IFS) has become a powerful tool in optical and infrared astronomy.[1] IFS enable us to obtain three–dimensional information (*i.e.* datacube) on position (x, y) and spectrum (λ) of astronomical objects such as galaxies, stars and interstellar medium. Thus, we can investigate spatially resolved physical properties or dynamical state (*e.g.* SFR, metallicity, velocity field, etc...) of above targets. Even though fabryperot interferometry or imaging fourier transform spectroscopy also offer a datacube as final products,[2] it is one of the advantage of using IFS that we can obtain it with only single exposure.

In particular, near–infrared IFS has further significance because they are less affected by dust attenuation and most of the key spectral features for deriving physical quantities are redshifted in the near–infrared at z > 1. In order to realize an integral field unit (IFU) for near–infrared wavelength, some technical challenges must be overcome. For example, optics should be put on cryogenic condition to reduce thermal emission. Therefore, there is a need to avoid mismatch of coefficient of thermal expansion between support structures and optical elements. And moreover, a field-of-view (FoV) has yet been limited because a detector for infrared application is too expensive to use as focal plane arrays compared with optical applications. Number of near–infrared IFUs have been increasing in this decade, however, it is still small compared with that of current optical IFUs. Moreover, efficient IFUs in terms of both FoV and spectral coverage are also needed to explore spatially resolved physical properties of astronomical targets.

Further author information: (Send correspondence to Y.K.)
Y.K.: E-mail: y_kitagawa@ioa.s.u-tokyo.ac.jp, Telephone: +81 422 34 5163

Advances in Optical and Mechanical Technologies for Telescopes and Instrumentation II,
edited by Ramón Navarro, James H. Burge, Proc. of SPIE Vol. 9912, 991225

doi: 10.1117/12.2231931

2. OVERVIEW OF SWIMS–IFU

SWIMS–IFU,[3,4] a module we have been developing, should be applicable to the requirements as described in Sec. 1. It will be integrated into the SWIMS spectrograph as a compact optical system and offer new capability to realize IFS observation easily on the Subaru and TAO telescope as follows.

2.1 SWIMS spectrograph

SWIMS (Simultaneous–color Wide–field Infrared Multi–object Spectrograph)[5,6] is near–infrared camera and multi–object spectrograph, which has been developed by Institute of Astronomy, Graduate School of Science, the University of Tokyo. It is one of the first–generation instruments for the University of Tokyo Atacama Observatory (TAO) 6.5-m telescope constructed at the world's highest astronomical site, the summit of Cerro Chajnantor (an altitude of 5,640 m) in northern Chile. SWIMS also plan to be mounted on the Cassegrain focus of the Subaru telescope and see the first light in 2016. All the components of SWIMS have been already manufactured and delivered, and performance verification of the whole system is currently in progress.[7,8]

For multi–object (or long–slit) spectroscopy mode, a carousel unit (*i.e.* a MOS–mask storage cryostat) located on a main cryostat keeps 20 slit masks under 80K. We can select an assigned mask for an observation program and remotely put it on the telescope focal plane by a mask exchanger unit.[9] A key feature of SWIMS spectrograph is capability of acquirement entire near–infrared spectrum from 0.9 to 2.5 μm by only one exposure. As shown in Fig. 1, SWIMS spectrograph has a dichroic mirror located in collimated beam and the mirror splits the incident light from the telescope into two–color (*blue*: 0.9-1.45 μm/ *red*: 1.45-2.5 μm). Each channel has a grizm and two or four HAWAII–2RG arrays in the phase of Subaru or TAO telescope respectively, so we can simultaneously obtain these spectra with one exposure.

2.2 IFS option for SWIMS

SWIMS was originally designed as conventional imager and multi–object spectrograph. Considering importance of near–infrared IFUs have been increasing as described in Sec. 1, we made the decision to have additional observation mode, SWIMS–IFU. It has a wider field coverage of $17'' \times 13''$ for the TAO 6.5m telescope, compared with

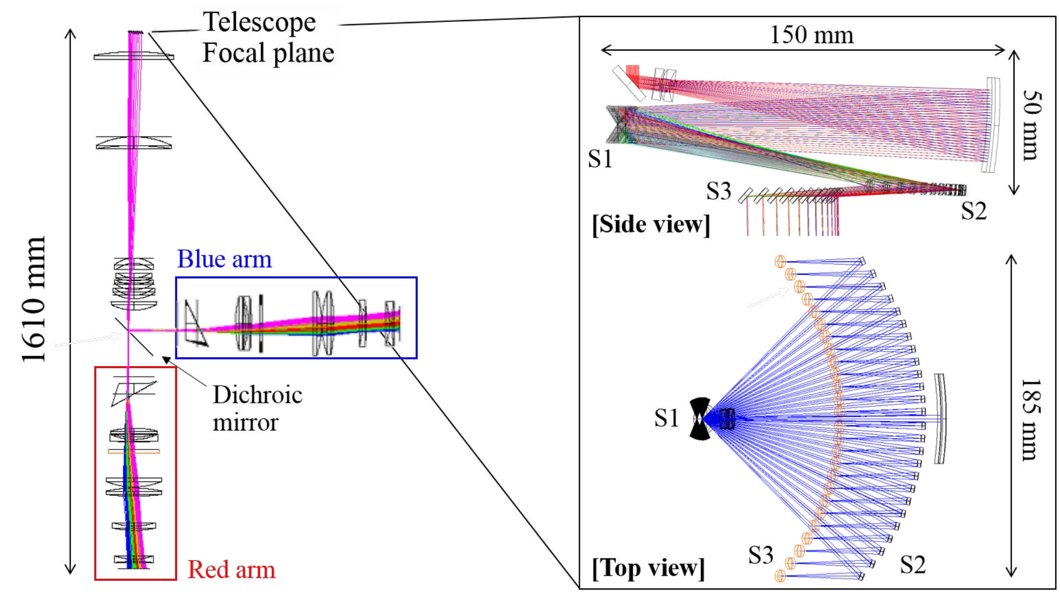

Figure 1. (*left*) A schematic illustration of whole optics inside SWIMS main dewar. The blue and red squares represent a spectrograph for 0.9–1.45 and 1.45–2.5 μm, respectively. The incident light from a telescope comes from upper left side of the image and is separated by the dichroic mirror. (*right*) A layout of the IFU optics in side view (from the direction perpendicular to the telescope optical axis) and in top view (from the direction to the telescope optical axis). We adopt the "Advanced Image Slicer" layout.[10]

current near–infrared IFUs whose FoV is typically smaller than 100 arcsec^2. The spectral coverage of SWIMS–IFU is also wider which covers whole near-infrared spectrum from 0.9 to 2.5 μm and we can simultaneously obtain these spectra by only one exposure as mentioned above.

In order to realize IFS observation with SWIMS we adopted concept of modularly-structured unit.[11] This means we only have to fabricate a hand-sized IFU module like a MOS slit mask which contains enlarger optics, an image slicer, a pupil mirror array and a slit mirror array (Fig. 1). And these optics don't impose any change on the existing SWIMS optics. Then IFS mode can be easily realized by just inserting the IFU module into the focal plane stage using the mask exchanger (see also Fig. 3). In the current design we were successful to make the size of the unit fall in a volume of 60 × 170 × 225 mm^3. Consequently, SWIMS–IFU have capability of efficient observation the Subaru and the TAO 6.5m telescope, which provides spatially resolved entire near–infrared datacube in wide FoV.

3. MECHANICAL STRUCTURE

3.1 Strategy for precision alignment

Alignment procedure is assumed to be pretty difficult due to a compact design of SWIMS–IFU. Mirror arrays have very complicated shape, which have many facets like image slicer. And each facet should be aligned with high accuracy about reference plane of system. In order to achieve high accurate alignment of IFU optics, we need actively to adopt monolithic fabrication of each optical surfaces from metallic alloy. For this purpose ultra–precision machining using a diamond tool is most suitable.[12] Compared with polishing process, cutting process has drawback in the terms of surface roughness. However, the degree of freedom of making surface figure and reducing machining time is even attractive for IFU application. So we adopted this technique for fabricating SWIMS–IFU optics.

We will monolithically fabricate not only each *facet* in mirror arrays, but also each *optical elements* in the unit. For example, conceptual design of the IFU is shown in Fig. 2 and same color means that the optical surfaces will be fabricated of a piece of alloy. Number of components can be dramatically reduced, thus there are only three-components (*i.e.* red, blue, and green one) to be aligned in the unit. The position of each optical surface in a component can be determined by processing accuracy. And degree of freedom of each large components is fixed by position–adjusting pins with thin spacer to adjust moderate offset. These strategy will realize high-precision alignment and help to reduce alignment process.

3.2 Load test using a dummy unit

Not only a size but a weight of the unit is also important factor. In order to confirm that grasping power of the mask exchanger is enough to handle the unit, we demonstrated a load test in March 2016. For this purpose, we

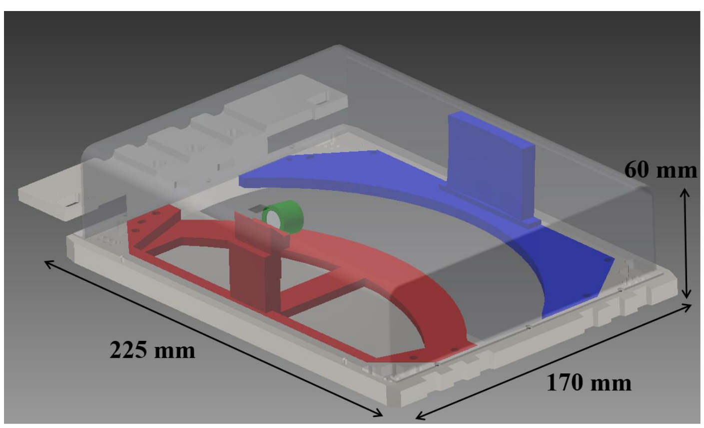

Figure 2. A CAD image of conceptual design of SWIMS–IFU. The size of the unit is 60 × 170 × 225 mm^3.The image is false-colored and the same color means *one* optical component (see Sec.3.1). A housing of the unit is made transparent for the purpose of illustration, and the actual parts will be painted in black in near–infrared to avoid stray light.

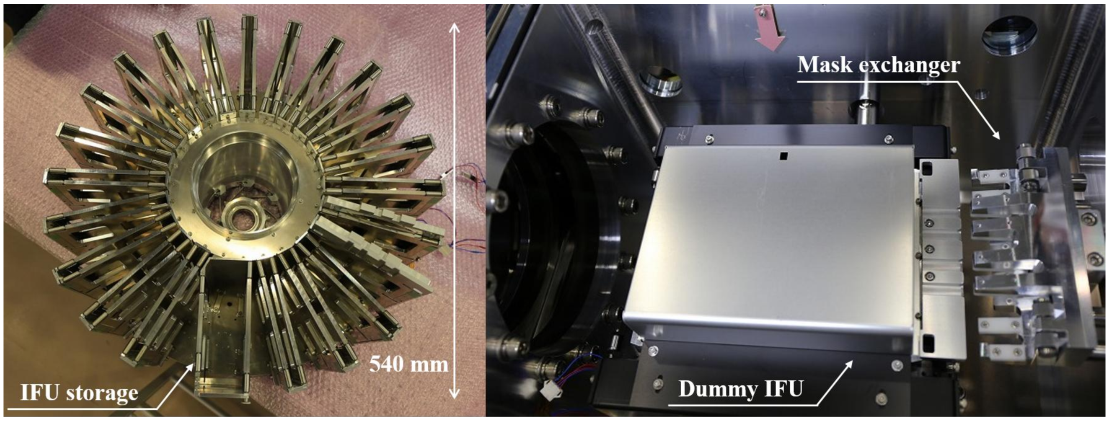

Figure 3. (*left*) A carousel unit as a storage for MOS slit masks. A larger housing at the bottom side in the picture corresponds to an IFU storage. (*right*) Focal plane stage inside a MOS dewar. The left side of the picture corresponds to the mask storage.

prepared a dummy unit which has same size of actual one and is adjusted its weight to design value $\sim$ 900 g. As shown in Fig. 3, the IFU storage occupies a volume corresponding to that of two-slit masks in the carousel. The position of the unit on the focal plane stage and inside the storage must be determined by neodymium magnets embedded in a baseplate of the unit.

Then we checked whether the exchanger handle the dummy unit between a IFU storage and the focal plane stage without any trouble in 100 times continuously. As the result of the test, we confirmed that design value of $\sim$ 900 g did not cause any problem at ordinary temperatures and pressures. The same procedure under cryogenic condition and under changing direction of gravitational force will be carried out as a next step.

4. MIRROR FABRICATION

As mentioned in Sec. 3 we need to investigate monolithic fabrications using ultra–precision cutting (UPC) technique. So we set up two goals in this study. One is to establish a method to monolithically make complicated mirror arrays using UPC technique. And the other is to apply this technique to manufacture IFU mirror arrays, especially image slicer. The experimental setup and its results are as follows.

4.1 Mirror material

To improve surface roughness we adopt electroless nickel–phosphorus (Ni–P) coatings by following reasons. First a roughness value of finished surface with electroless Ni–P often shows less than 10 nm r.m.s using diamond cutting. It is enough to our application to near–infrared observations. And it is easy to maintain surface quality thanks to high hardness of Ni–P compared with that of raw metals such as an aluminum or an oxygen-free copper. Also Ni–P coated surface can be polished, therefore cutting marks can be erased if we establish micro–polishing technique which could be applicable to multi–faceted mirror arrays. Of course, there remains a problem that mismatch of the coefficient of thermal expansion (CTE) between base and coating materials must be resolved. To solve this, we employ special aluminum alloy which has the CTE almost same as that of electroless Ni–P over a wide temperature range.[13] All the components in SWIMS–IFU such as optical elements and support structure will be planned to made of the CTE–matched aluminum.

Note that fabrication experiment in following sections are performed by using a conventional aluminum alloy (*i.e.*A5052) coated with Ni–P. This fact does not affect the following results, however, because values of surface roughness could be dependent on properties of not base material but coating material, and all measurements of surface figure were performed at room temperature.

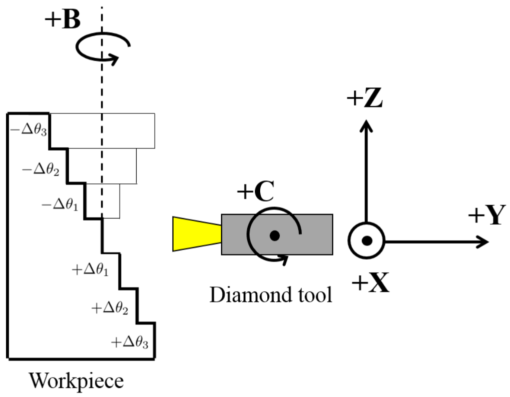

Figure 4. A schematic illustration of assignment of degrees of freedom of the ultra–precision machine. "+" sign means that a corresponding plane are tilted along B-axis with positive angle (*e.g.* $+\Delta\theta_1 < +\Delta\theta_2 < +\Delta\theta_3$).

4.2 Setup of fabrications

We fabricated test pieces of an image slicer as a proof-of-concept experiment to find best way of manufacturing a multi–faceted mirror. The test slicers have 25 reflective planes whose width is 500 μm and angular difference between adjacent facets is $\sim$ 0.4 degrees (see also Fig. 5). Each reflective plane has flat surface form and has no tilt angle along slicing direction. These specifications are slightly simplified to test fabrications, but are almost same as them for science observations. Requirements for surface roughness and figure error are less than 10 nm r.m.s. and 100 nm P–V, respectively. These value should not be difficult in a case of single surface optics. However, it is a kind of hard target for a multi–faceted mirror such as an image slicer.

In this experiment two approaches were adopted to create surface figure, one is milling process and the other is shaper cutting process. We used both 4-axis and 5-axis ultra-precision machines at the RIKEN Center for Advanced Photonics for the former and the later process, respectively. A schematic illustration in Fig. 4 shows how to assign degrees of freedom of the machine to a configuration of a diamond tool and a workpiece. A diamond tool can move freely along X, Y,and Z directions and a rotation axis assigned to workpiece make surface figure multi–faceted. In addition, a rotation axis assigned to a diamond tool was used in shaper cutting process in order not only to adjust tool position but also to make surface figure tilted along slicing direction (this application was not used in the following experiments). In both of these process, we prepared custom-made diamond tools. In milling process, a diameter of square end mill is ϕ 500 μm, and it was used with rotating speed of 15,000 r.p.m. and feed rate of 50 mm/min. On the other hand a nega–tapered flat blade whose width is also 500 μm was used in the shaper cutting process with feed rate of 1,000 mm/min.

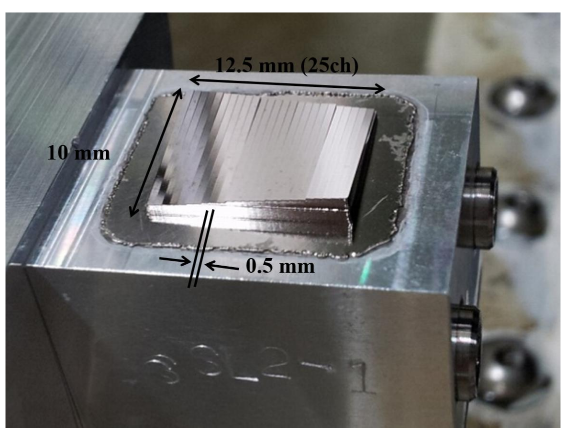

Figure 5. A picture of finished surface of a test piece.

A work flow of fabrication of image slicer as follows: First we prepared a blank aluminum block and carried out near net shape machining in order to reduce machining time in post–process . Then whole surface is coated by electroless Ni–P with thickness of 100 μm. Finally surface finish is performed by milling process or shaper cutting process. A conventional machining center are used in pre-process and a ultra–precision machine are used only in the final step.

4.3 Results

In the milling process, a measurement results of surface roughness taken by white–light interferometer is shown in Fig. 6. The roughness value evaluated over the region of 500 μm $\times$ 700 μm is $\sim$ 63 nm. There can be seen not only cutting marks of milling in 2–D surface profile, but hyperbolic–curved cross section in 1–D profile along slicing direction. This hyperbolic shape could be caused as the result of misalignment between the diamond tool and the translational axis of the machine. Corresponding angular offset value from ideal position is $\sim$ 0.02 deg, and we can correct it by modifying tool path with simultaneous control of 2–axis. Obviously this global feature make a large influence on evaluation of roughness. Thus this the deviation from ideal surface form results large figure error and roughness value. So we fitted the surface form and removed the cylindrical component from the original data in order to estimate actual roughness value. Then, as shown in Fig. 7, we obtained the evaluated value of 11 nm. This value almost reaches our requirements for near-infrared observations. We adopted this value as a benchmark of practical roughness when using milling processing.

In the shaper cutting process, results of roughness measurement are shown in Fig. 8. Surface profile shows different feature compared with milling process, and we obtained almost flat surface. This satisfies the requirement for figure error and also shows good surface roughness which achieves 9.7 nm r.m.s.. Unfortunately there can be seen lines along cutting direction whose height are $\sim$ 40 nm at the center of the 2–D profile. These feature are due to chips on a edge of diamond tool. Although, these measurement results shows the shaper cutting process satisfies our requirements.

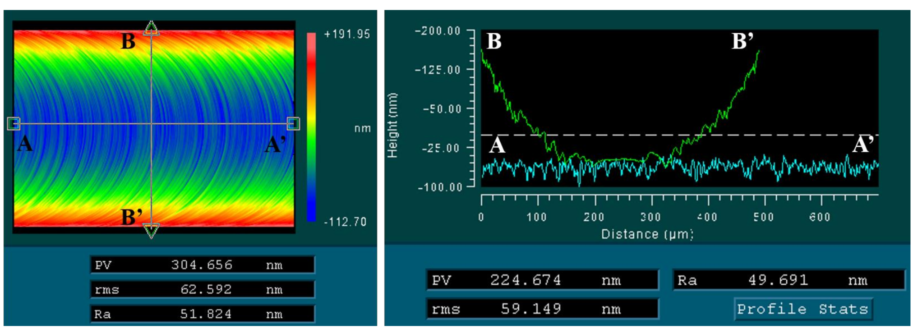

Figure 6. (*left*) A roughness measurement of a reflective plane finished by milling process. A direction of processing is from A to A'. (*right*) A profile of cross-section corresponding to a line $[A–A']$ and $[B–B']$ in the left panel.

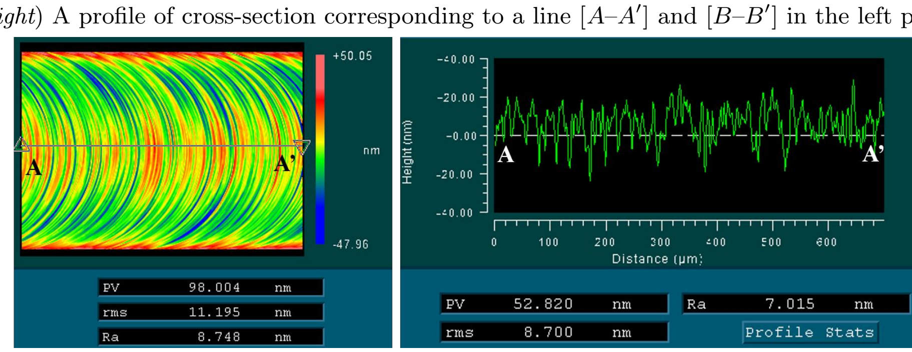

Figure 7. Same as Fig. 6, but the *cylindrical* component is numerically pre–subtracted from original data of Fig. 6 before calculation of roughness.

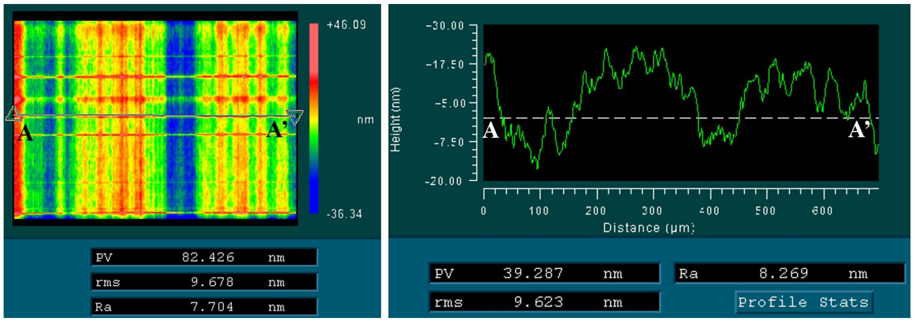

Figure 8. Same as Fig. 6, but the result for shapar cutting process. A tilted component is corrected before calculation of roughness.

Table 1. Summary for experimental results

	Requirements	Milling process	Shaper cutting process
Surface roughness	< 10 nm	11 nm	9.7 nm
Figure error	< 100 nm	300 nm	82 nm
Setting	——	~ 1 day	2 days
Machining time (25 ch)	——	~ 3 hours	0.5 hours

The measurement results of the fabrication experiments are summarized in Table 1. When comparing both of two methods, we can find the shaper cutting process is one of the best way to fabricate an image slicer in terms of both surface roughness and figure error. Of course this result does not mean the milling process cannot be available for manufacturing an image slicer. Performing test cutting previously, we can estimate deviation of tool position and correct hyperbolic–curved surface form by calibrating tool path with simultaneous control of 2–axis. After that, surface roughness will potentially achieve less than 10 nm gathered from the result in Fig. 7.

Through this proof-of-concept experiments, we have established a method to manufacture complicated mirror arrays using ultra-precision cutting technique. And the measurement results showed shaper cutting process will be one of the good way to fabricate an image slicer.

5. SUMMARY AND FUTURE TASKS

In this study, we investigated how to manufacture IFU mirror arrays, especially image slicers, using diamond cutting technique. And we found shaper cutting process is suitable for fabricating image slicers. The measurement results taken by white–light interferometer show that the surface roughness is almost satisfies our requirement in both of two methods. Moreover, we obtained ideal surface form in shaper cutting process, too. This method will be adopted to other mirror arrays such as pupil mirror and slit mirror, and this monolithic fabrications also help us to considerably reduce alignment procedure of each optical elements. As next step, we need further investigation in order to apply this process to other IFU mirror arrays.

SWIMS will be transfered to the NAOJ Hawaii observatory and see the engineering first light on the Subaru telescope in 2016 winter. Regarding the SWIMS-IFU, we have finished optical and mechanical design and plan to perform fabrications of all the optical and structure components. After assembling components of optical elements and confirmation its performance in the laboratory in Japan, SWIMS–IFU will be transported to the observatory and be integrated in the carousel unit of SWIMS. The first light of IFS mode of SWIMS spectrograph will be carried out in 2017.

ACKNOWLEDGMENTS

This research is funded by a supplementary budget for economic stimulus packages formulated by Japanese government. Part of the development is supported by Ministry of Education, Culture, Sports, Science and

Technology of Japan, Grant-in-Aid for Scientific Research (15H02062, 23540261, 24103003, 24244015, 2611460, and 266780) from the JSPS of Japan, and by the grant of Joint Development Research supported by the Research Coordination Committee, National Astronomical Observatory of Japan (NAOJ). The development activities are supported by the Advanced Technology Center, NAOJ.

REFERENCES

[1] Kissler-Patig, M., Walsh, J. R., and Roth, M. M., eds., [*Science Perspectives for 3D Spectroscopy*] (2007).

[2] Eisenhauer, F. and Raab, W., "Visible/Infrared Imaging Spectroscopy and Energy-Resolving Detectors," *Annual Review of Astronomy and Astrophysics* **53**, 155–197 (2015).

[3] Ozaki, S., Kitagawa, Y., Motohara, K., Konishi, M., Takahashi, H., Yoshikawa, T., Tateuchi, K., and Kato, N., "Development of an integral field unit for a near-infrared multi-object imaging spectrograph SWIMS," *Proceedings of the International Society for Optical Engineering* **8450**, 84503Y (2012).

[4] Kitagawa, Y., Ozaki, S., Motohara, K., Konishi, M., Takahashi, H., Tateuchi, K., Todo, S., Kato, N., and Yoshikawa, T., "Concept and optical design of the near-infrared integral field unit for SWIMS," in [*Advances in Optical and Mechanical Technologies for Telescopes and Instrumentation*], *Proceedings of the International Society for Optical Engineering* **9151**, 91514P (2014).

[5] Konishi, M., Motohara, K., Takahashi, H., Tateuchi, K., Kitagawa, Y., Kato, N., Aoki, T., Doi, M., Handa, T., Kamizuka, T., Kawara, K., Kohno, K., Koshida, S., Minezaki, T., Miyata, T., Morokuma, T., Sako, S., Soyano, T., Tamura, Y., Tanabe, T., Tanaka, M., Tarusawa, K., and Yoshii, Y., "Design and development of SWIMS: a near-infrared multi-object spectrograph for the University of Tokyo Atacama Observatory," in [*Ground-based and Airborne Instrumentation for Astronomy IV*], *Proceedings of the International Society for Optical Engineering* **8446**, 84467P (2012).

[6] Motohara, K., Konishi, M., Takahashi, H., Tateuchi, K., Kitagawa, Y., Todo, S., Kato, N. M., Ohsawa, R., Aoki, T., Asano, K., Doi, M., Kamizuka, T., Kawara, K., Kohno, K., Koshida, S., Minezaki, T., Miyata, T., Morokuma, T., Okada, K., Sako, S., Soyano, T., Tamura, Y., Tanabe, T., Tanaka, M., Tarusawa, K., Uchiyama, M., and Yoshii, Y., "Development of a simultaneous two-color near-infrared multi-object spectrograph SWIMS for the TAO 6.5-m telescope," in [*Ground-based and Airborne Instrumentation for Astronomy V*], *Proceedings of the International Society for Optical Engineering* **9147**, 91476K (2014).

[7] Motohara, K., Konishi, M., Takahashi, H., Kato, N. M., Kitagawa, Y., Kobayakawa, Y., Terao, Y., Ohashi, H., Aoki, T., Doi, M., Kamizuka, T., Kohno, K., Minezaki, T., Miyata, T., Morokuma, T., Mori, K., Ohsawa, R., Okada, K., Sako, S., Soyano, T., Tamura, Y., Tanabe, T., Tanaka, M., Tarusawa, K., Uchiyama, M., Koshida, S., Asano, K., Tateuchi, K., Uchiyama, M., Todo, S., and Yoshii, Y., "NIR camera and spectrograph SWIMS for TAO 6.5m telescope : Overview and development status," in [*Ground-based and Airborne Instrumentation for Astronomy VI*], *Proceedings of the International Society for Optical Engineering*, in press (2016).

[8] Terao, Y., Motohara, K., Konishi, M., Takahashi, H., Kato, N., Kitagawa, Y., Kobayakawa, Y., Ohashi, H., Tateuchi, K., and Todo, S., "NIR camera and spectrograph SWIMS for TAO 6.5m telescope: array control system and its performance," in [*High Energy, Optical, and Infrared Detectors for Astronomy VII*], *Proceedings of the International Society for Optical Engineering*, in press (2016).

[9] Takahashi, H., Konishi, M., Motohara, K., Kato, N. M., Tateuchi, K., Kitagawa, Y., and Todo, S., "Development of multi-object spectroscopy unit for simultaneous-color wide-field infrared multi-object spectrograph," in [*Ground-based and Airborne Instrumentation for Astronomy V*], *Proceedings of the International Society for Optical Engineering* **9147**, 91476N (2014).

[10] Content, R., "New design for integral field spectroscopy with 8-m telescopes," in [*Optical Telescopes of Today and Tomorrow*], Ardeberg, A. L., ed., *Proceedings of the International Society for Optical Engineering* **2871**, 1295–1305 (1997).

[11] Allington-Smith, J. R., Content, R., Dubbeldam, C. M., Robertson, D. J., and Preuss, W., "New techniques for integral field spectroscopy - I. Design, construction and testing of the GNIRS IFU," *Monthly Notices of the Royal Astronomical Society* **371**, 380–394 (2006).

[12] Dubbeldam, C. M., Clark, P., Content, R., Kirby, A. K., Parkin, K., Robertson, D. J., Rolt, S., Ryder, D. A., and Sharples, R. M., "The KMOS Integral Field System: fabrication, alignment, and test of 1000+ optical surfaces," in [*Modern Technologies in Space- and Ground-based Telescopes and Instrumentation II*], *Proceedings of the International Society for Optical Engineering* **8450**, 84501M (2012).

[13] Kinast, J., Hilpert, E., Lange, N., Gebhardt, A., Rohloff, R.-R., Risse, S., Eberhardt, R., and Tünnermann, A., "Minimizing the bimetallic bending for cryogenic metal optics based on electroless nickel," in [*Advances in Optical and Mechanical Technologies for Telescopes and Instrumentation*], *Proceedings of the International Society for Optical Engineering* **9151**, 915136 (2014).